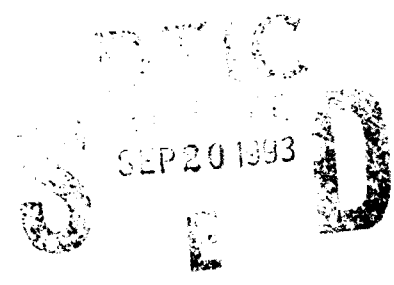AD-A270 100

# SURFACE WAVE GROUP VELOCITY TOMOGRAPHY OF EAST ASIA

Francis T. Wu

State University of New York
Department of Geological Sciences
and Environmental Studies
PO Box 6000
Binghamton, NY 13902-6000

July 25, 1993

SEP 20 1993

**PHILLIPS LABORATORY**
Directorate of Geophysics
**AIR FORCE MATERIEL COMMAND**
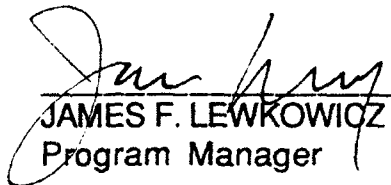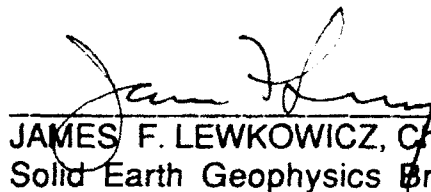**HANSCOM AIR FORCE BASE, MA 01731-3010**

93 9 17 004

93-21676

The views and conclusions contained in this document are those of the authors and should not be interpreted as representing the official policies, either expressed or implied, of the Air Force or the U.S. Government.

This technical report has been reviewed and is approved for publication.


JAMES F. LEWKOWICZ
Program Manager

JAMES F. LEWKOWICZ, Chief
Solid Earth Geophysics Branch


DONALD H. ECKHARDT, Director
Earth Sciences Division

# REPORT DOCUMENTATION PAGE

Public reporting burden for this collection of information is estimated to average 1 hour per response, including the time for reviewing instructions, searching existing data sources, gathering and maintaining the data needed, and completing and reviewing the collection of information. Send comments regarding this burden estimate or any other aspect of this collection of information, including suggestions for reducing this burden, to Washington Headquarters Services, Directorate for Information Operations and Reports, 1215 Jefferson Davis Highway, Suite 1204, Arlington, VA 22202-4302, and to the Office of Management and Budget, Paperwork Reduction Project (0704-0188), Washington, DC 20503

| 1. AGENCY USE ONLY (Leave blank) | 2. REPORT DATE July 25, 1993 | 3. REPORT TYPE AND DATES COVERED Final Part I  Feb. 1, 1992–Feb. 1, 1993 |
|---|---|---|

**4. TITLE AND SUBTITLE**

Surface Wave Group Velocity Tomography of East Asia

**6. AUTHOR(S)**

Francis T. Wu

**5. FUNDING NUMBERS**
PE 62101F
PR 7600 TA 09 WU AR

Contract F19628-90-K-0042

**7. PERFORMING ORGANIZATION NAME(S) AND ADDRESS(ES)**

State University of New York
Department of Geological Sciences and Evironmental Studies
PO Box 6000
Binghamton, NY 13902-6000

**8. PERFORMING ORGANIZATION REPORT NUMBER**

**9. SPONSORING/MONITORING AGENCY NAME(S) AND ADDRESS(ES)**

Phililips Laboratory
29 Randolph Road
Hanscom AFB, MA 07131-3010

Contract Manager: James Lewkowicz/GPEH

**10. SPONSORING/MONITORING AGENCY REPORT NUMBER**

PL-TR-93-2102 (I)

**11. SUPPLEMENTARY NOTES**

**12a. DISTRIBUTION/AVAILABILITY STATEMENT**

Approved for Public Release;
distribution unlimited

**12b. DISTRIBUTION CODE**

**13. ABSTRACT (Maximum 200 words)**

Group velocities of both Rayleigh and Love waves are used in a tomographic inversion to obtain group velocity maps of East Asia ($60^\circ$E–$140^\circ$E and $20^\circ$N–$50^\circ$N). The period range studied is 30–70 seconds. For periods longer than 40 seconds, a high group velocity gradient clearly exists along longitude $105^\circ$E; the velocities are noticeably higher east of this longitude than west of this longitude. The Tibetan Plateau appears as a prominent low velocity (about –15%) structure in this area; central Tibet appears as the area with the lowest velocity. The North China Plain is an area of high velocities, probably as a result of thin crust. The variability of deep crustal and upper mantle structures underneath the different tectonic provinces in the study area can clearly be seen.

In a separate study, using the dataset above and that from the former Soviet Union, we have derived the Rayleigh tomographic images of a larger area ($40^\circ$E – $160^\circ$E and $20^\circ$N–$70^\circ$N). While the Tibetan plateau still remains to be the most prominent low velocity features, two other features are also clear, a very high velocity Siberian platform and a high velocity ridge extending from Lake Baikal to Central Mongolia. These studies are useful in delineating tectonics.

**14. SUBJECT TERMS**

Seismology, surface waves. tomography, Asia

**15. NUMBER OF PAGES**
50

**16. PRICE CODE**

| 17. SECURITY CLASSIFICATION OF REPORT | 18. SECURITY CLASSIFICATION OF THIS PAGE | 19. SECURITY CLASSIFICATION OF ABSTRACT | 20. LIMITATION OF ABSTRACT |
|---|---|---|---|
| Uncladdified | Unclassified | Unclassified | SAR |

NSN 7540-01-280-5500

# Table of Contents

# Surface Wave Group Velocity Tomography of East Asia

## Introduction

The East Asian continent grew throughout the geological ages as a result of successive accretions of younger terranes onto a geologically ancient (Archean) core, the Siberian platform (e.g., Yang et al., 1986). Figure 1 shows that around the core there are several Pre-Cambrian geological terranes, the Ordos, the Tarim and the Ala Shan blocks. The Late Paleozoic and Mid-Mesozoic South China Block was most probably accreted to the continent in Late Paleozoic and the Tibetan Block was attached to the continent in Mid- to Late Mesozoic. In between these older blocks were Paleozoic collision zones (the Tienshan, the Nan-shan and the A-erh-chin Shan [Altyn Tagh] Fold Belts). The impingement of the Indian plate along the Himalayan front that started about fifty million years ago had led to the formation of Tibet and the ongoing continental tectonics of the whole East Asian area. While some of the ancient blocks, for example, the Tarim and Ordos, remain mostly passive, the fold belts were reactivated and became the locus of recent active tectonics. The earthquakes in this area were some of the most energetic among the continental events; the primary tectonic stress is thought to come from the collision south of Tibet (Molnar and Tapponier, 1978).

The tectonic units shown in Figure 1 are drawn mainly on the basis of surface geology; some of the major units are also clearly discernible as major topographical features (Figure 2). But some of the major topographical features are not clearly expressed in the tectonic map. For example, in Figure 1 Tienshan is shown to continue southeastward of WMQ station, but Tienshan actually changes there from high mountain ranges southwest of WMQ to E-W oriented basin and ranges, with an extensive topographic low (Figure 2). The lowest point is in the Turfan basin (-154 m). Is there a corresponding expression in the crustal and mantle structures? One also wonders whether there is any common deep structural expressions of the ancient blocks mentioned earlier. Judging from the gradational changes of topography from western China to

1

eastern China (Figure 2), there may also be a corresponding regional change in crustal and upper mantle velocity structures. As far as the Tibetan plateau is concerned, since the manner in which the Tibetan topography is supported and the processes that led to its formation must be related to the deep structure under the plateau, velocity structures under the plateau as well as how the structures in the surrounding areas vary provide key information for the contemporaneous tectonics of the region. We conducted this surface wave tomographic study of Eastern Asia to investigate the large scale lateral velocity variations in this area.

Reflection and refraction profiles provide the most detailed look of crustal structures of an area. A limited number of crustal reflection and refraction profiles in various parts of China (see Wang and Mao, 1985, for a summary) have been published. By far, the most detailed surveys were done in North China Plain, near Beijing, in conjunction with earthquake studies. Elsewhere there are one or two refraction lines in a large area, such that the overall thickness of the crustal thicknesses are known. Several refraction and wide-angle reflection studies were done in southern Tibet (Wang and Mao, 1985; Him, 1988). The lateral extent of the plateau, the changes in velocity and crustal thickness within the plateau were not mapped by such studies.

Surface waves from earthquakes, with a wide period range, can be used to obtain average structures along their travelling paths or tomographic inversion. With the exception of a two-station dispersion study by Feng et al. (1983), and a tomographic study of Tibet by Bourjot and Romanowicz (1992), most of the previous surface wave studies in East Asia were done with data external to the region of interest. Feng et al. (1983) used data recorded on Kirnos seismographs from stations within China to derive Rayleigh wave dispersion in the period range of 10 to 50 seconds. Relatively few paths were used in their study. Patton (1980) and Feng and Teng (1983) obtained dispersion curves for various areas of Eurasia with Rayleigh waves traversing through the area by regionalization; while Patton (1980) defined the sub-regions based on topography and known crustal thickness, Feng and Teng (1983) divided the region into 10° x 10° grid. Velocity structures for the resolved regions were then determined through inversion. Chun and Yoshii (1977) used events on the eastern side of the plateau and stations south of the Himalayas; they aim their study at Tibet. Brandon and Romanowicz (1986) employ the "two-event" technique to determine dispersion curves in northern Tibet. Kozhevnikov and Barmin (1989) ana-

2

lysed about 200 records of analog Soviet stations and several SRO stations deployed in Asia to obtain average Rayleigh wave group velociy curves for several apriori determined tectonic regions of Eastern Asia. These curves were used by Kozhevnikov et al. (1992) to find average lithosphere shear velocity structure for Tibet, the mountain region of Southern Siberia and Mongolia, platforms of South-eastern China and some other regions. Bourjot and Romanowicz (1992) recently presented tomographic images of the Tibetan Plateau and its vicinity; they used two stations internal to China and several SRO stations in Asia and also ANTO in Turkey, GRFO in Germany and SSB in France.

For large scale lateral variations in crustal structures, the Bouguer gravity map of East Asia (USAF, 1971) provides a very good view (Figure 3). The most prominent anomalies on this map are on the Tibetan plateau, where the anomalies are as low as -550 mgal. The overall trend of anomalies shown on the map is the decrease in the amplitude of the negative anomalies toward the east. More details of this map will be discussed when comparisons of the map are made with our results.

As a result of the establishment of high quality seismic stations in China and its vicinity, the area can now be studied in more detail. The networks are still too sparse, with station spacing on the order of 1000 km. The data, however, does provide an adequate basis for tomographic imaging of the region as a whole. In this paper, we present the result of a tomographic study using group velocities recorded at six of the Chinese Digital Seismic Network (CDSN) and three Seismic Research Observatory (SRO) stations (see Figure 2 for station distribution). Our primary purpose in this work is to obtain an image, in terms of group velocity, of the laterally heterogeneous crustal and upper mantle structures of eastern Asia. Group velocity is used because we want to maximize our paths for better resolution and most of the events are too small to have dependable focal mechanisms.

We have available also, through Prof. Anatoli Levshin a group velocity dataset determined by Dr. V. M. Kozhevnikov, using stations from the former Soviet Union and China. By combining this and the CDSN/SRO dataset we can enlarge the area investigated. The preliminary results will be shown in this report.

The methodology used in our tomographic inversion was developed by Ditmar and Yanovskaya (1987; see also Levshin and Yanovskaya, 1989). For each period, a smooth group velocity distribution of the area is covered by the raypaths, with its resolution (in km) depending on the distribution of paths. The tomographic images of the region as a whole using Rayleigh and Love wave dispersion curves show clearly the lateral variations in crustal and upper mantle structures. Although Tibet is by far the most prominent feature in the region, we are able to resolve many smaller features as well in East Asia.

The tomographic results for the smaller dataset centered around China have been submitted for publication (Wu and Levshin, 1993). Results for the combined dataset will be submitted for publication, jointly with Dr. Anatoli Levshin after some more tests and interpretation are completed. Initial results will be reported at the Spring AGU, 1993 (Levshin, Wu and Kozhevnikov, 1993).

## Data

Figure 2 shows the locations of the CDSN and SRO stations and many of the events used in this study. Because of the wide dynamic range of the CDSN and the updated SRO seismic systems, although the records stay on scale for magnitude 7 earthquakes, surface waves from $M_S \sim = 4.3$ can often be used to determine group velocities in the 20-70 seconds range. Altogether 100 events, that occurred in 1987, first six months of 1989, 1990 and first half of 1991, were used; the time span was related to the availability of data when they were acquired. The events chosen are located in and around the study area are used. Of the 500 event-station paths, approximately 360 Love and 360 Rayleigh dispersion curves were retained for the final analyses. The group velocity dispersion curves were determined with an interactive multiple filter group velocity program on a workstation, allowing rapid group velocity determination and visual quality control. Dispersion data are discarded when the sonogram shows complex envelop structures along the group arrival. In such cases we note that the waveform is usually more complex and relatively small; such waves are probably radiated near the radiation pattern minimum and thus multipathing effects become pronounced.

4

Because of the relatively short path length used in our study, the effect if instrument group delay is not negligible in the determination of group velocities. McCowan and Lacoss (1978) have shown that SRO instruments have delays ranging from about 12 seconds at 20 seconds to about 24 seconds at 70 seconds (without anti-aliasing filter). For the CDSN long period channels the group delays ranges from 15 seconds at a period of 20 seconds to 35 seconds at a period of 30 seconds. With the path lengths varying from 1000 to 4000 km, neglecting group delays can lead to an error of several percent to ten percent. Figure 4 summarizes the group delays of the SRO, CDSN and the modified SRO instruments (MAJO2) used in this study.

We have recently, in cooperation with Anatoli Levshin of University of Colorado, joined the dataset we have obtained using CDSN and SRO stations with analog stations from the former Soviet Union and inverted for wider area tomography. The data are from these stations use a mixture of instruments, including the intermediate period Kirnos seismometers. The station locations are shown in figures displaying the results. The total number of paths used in this combined study is in excess of 1200.

## Tomographic Methodology

To invert surface wave group velocities we applied a technique developed by Ditmar and Yanovskaya (1987) and Yanovskaya and Ditmar (1990). This technique can be considered a generalization of the Backus-Gilbert inversion method (Backus and Gilbert, 1968, 1970) for 2D problems. Input data for inversion are group travel times $t_j$ for several fixed values $T_m$, $m = 1,...,M$, of period $T$ along given paths $L_j$, $j = 1,...,J$, and corresponding cross-correlation matrices of travel time errors $R_t |_{T=T_m}$. Results of inversion are maps of group velocity distribution $U(\theta,\phi) |_{T=T_m}$ and a map of space resolution $R(\theta,\phi)$ for a given set of paths. Here $\theta$ and $\phi$ are latitude and longitude, respectively. The inversion procedure will be repeated for each period of interest.

Let the real distribution of group velocities be $U_e(\theta,\phi)$. To get a tomographic image of it we use a laterally homogeneous initial model of the area $S$ under study with a constant group velocity $U_0$. The basic assumptions of the inversion technique are as follows:

i) Deviations of the real distribution of velocities from the starting model are small, i.e.,

5

$$m_e(\theta, \phi) = (U_e^{-1}(\theta, \phi) - U_0^{-1})U_0 \ll 1 \tag{1}$$

so that we can ignore the deviations of wave paths from great circles and, also, use linearized inversion procedures.

ii) Taking into account incompleteness and inaccuracy of the data set we are looking for a smooth image $m(\theta, \phi)$ of the real velocity perturbations relative to the starting model. To do this we introduce constraints

$$\int_S |\nabla m(r)|^2 \, dr = \min \tag{2}$$

and

$$\left(\frac{\partial m}{\partial n}\right)_{C_S} = 0. \tag{3}$$

Here $C_S$ is a contour surrounding the area $S$ and $n$ is a normal to $C_S$.

iii) The solution obeys constraints related to data

$$\int_S G_i(r)m(r)dr = \int_{L_i} m(s)U_0^{-1}ds = \delta t_i, \tag{4}$$

$$t_{0i} = \int_{L_i} U_0^{-1}ds. \tag{5}$$

Here $G_i$ is a data kernel singular along the path $L_i$, equal to zero outside the path and obeying the relation

$$\int_S G_i(r)dr = t_{0i} \tag{6}$$

$$\delta t_i \cong t_i - t_{0i} = \int_{L_i} m(s)U_0^{-1}ds. \tag{7}$$

Using the regularization technique (Tikhonov and Arsenin, 1976) in the case of inaccurate data it is possible to state the problem of searching for a solution as finding the minimum of the following functional

6

$$(\delta t - P)^{T} \cdot_t^{-1}(\delta t - P) + \alpha \int_S |\nabla m(r)|^2 \, dr = \min \tag{8}$$

Here $P_i = \int_S G_i(r)m(r)dr$ and $\alpha$ is a regularization parameter. $\alpha$ must be chosen so that the

first term in (8) is equal to the total number N of data. By increasing $\alpha$ we impose stronger

smoothness and decrease the resolving power of data.

The solution $m(\theta, \phi)$ is found using formulas:

$$m = A^T \delta t, \tag{9}$$

where

$$A^T = K^T(S + \alpha R_i)^{-1} = \frac{1 - K^T(S + \alpha R_i)^{-1}t_0}{t_0^T(S + \alpha R_i)^{-1}t_0} t_0^T(S + \alpha R_i)^{-1} \tag{10}$$

$$K_j(r) = \int_{L_j} \ln |r - r_j| \frac{ds_j}{U_0} \tag{11}$$

$$S_{ij} = \int_{L_i} \int_{L_j} \ln |r_i - r_j| \frac{ds_i}{U_0} \frac{ds_j}{U_0}. \tag{12}$$

Space resolution is determined using formula

$$R = \exp(3/4 - A^T S A + 2K^T A). \tag{13}$$

Derivation of (9-13) is given by Ditmar and Yanovskaya (1987); see also Levshin et al. (1989).

The inversion proceeds by several steps:

1. Transformation from spherical to Cartesian coordinates:

   Transformation from spherical coordinates $\theta, \phi$ to Cartesian coordinates $x, y$ is done by using

formula (Yanovskaya, 1982; Jobert and Jobert, 1983):

$$x = R_0 \ln \tan(\theta/2), \tag{14}$$

$$y = R_0 \phi, \tag{15}$$

$$U(x, y) = U(\theta, \phi)/\sin\theta, \tag{16}$$

where $R_0$ is the Earth's radius. This transformation does not distort a velocity distribution if the latitude $\theta$ is not very high. To make this transformation more accurate the Earth's standard geocentric coordinate system is transformed first by rotation in such a way that the new equator crosses the middle of the territory under study and the new latitude range of wave paths is narrower than the real one. Several trials have demonstrated that reasonable variations of the new equator's position do not change results of inversion.

Then for a given period $T_m$:

2. For each $T_m$ the starting value of a group velocity $U_0$ is found as an average along all paths

$$U_0 = \frac{\sum_{J=1,J} D_J}{\sum_{j=1,J} t_j} \tag{17}$$

Here $D_j$ is a length of the path $L_j$.

3. Functions $U(\theta, \phi)$ and $R(\theta, \phi)$ are found using (9-13) and transformed to initial coordinate system.

4. Steps 2-3 are repeated with different values of the regularization parameter. There is an option in inversion procedure taking into account the presence of an azimuthal anisotropy in the Earth's model. The group velocity model is constructed as a function of coordinates $\theta, \phi$ and azimuth $\psi$

$$U_{anis}(\theta, \phi, \psi) = U(\theta, \phi)(1 - B \sin 2\psi). \tag{18}$$

The angle $\psi$ and coefficient $B$ are determined for each point.

## Tomographic results for $20°N \, to \, 50°N$ and $60°E \, to \, 140°E$

The path coverage we are able to obtain with our present dataset is shown in Figure 5. The total number of paths used for each tomographic inversion, the corresponding initial group velocities and the mean square residuals for resulting models are presented in Table I. Figures 6a-e and 7a-e show the tomographic results for Rayleigh and Love waves, respectively, at 30, 40, 50, 60 and 70 second periods. To maximize the color contrast for each figure, we have chosen to set

8

the minimum group velocity of each figure to red and the maximum to purple in the rainbow color scale. The map projection parameters used for these and the topography map (Figure 2) are identical, and they can thus be easily compared. For the tectonic and the Bouguer anomalies the coordinates and the location of the stations make the comparison of these maps possible. When viewing these maps it is important to keep in mind the following four factors. First, the resolution maps shown in Figure 6f and Figure 6f, for Rayleigh and Love waves respectively; in either case, the resolution of our tomographic results is on the order of 450-700 km in the central part of the map and increases sharply toward the edge, where the path coverage is poor (Figure 5). Secondly, since these are maps of differences in group velocities, they cannot be interpreted in terms of velocity structure differences; for example, low group velocities may arise from a combination of relatively low velocities in the vertical column and a thick crust. Thirdly, the horizontal wavelength corresponding to 30-70 second waves are approximately 95-280 km, and the image is expected to be smoother for longer periods. Finally, because Rayleigh and Love waves have different eigenfunctions (Figure 8), they sample the Earth differently even for an iso-tropic layered Earth; we do not expect the images for these two waves at the same period to be identical. All results described above were obtained assuming an isotropic model of the territory under study. Inversion taking into account the presence of anisotropy results in a model with 2% variations of velocity with azimuth. The strike of maximum velocity direction strike is equal to 68°. This model produces practically the same group velocity maps and average residuals as the isotropic one. We conclude that the given set of data does not indicate presence of significant azimuthal anisotropy of surface wave group velocities in the investigated regions.

The group velocity variations are remarkably different in different parts of the study area. To facilitate our description of the maps, we shall divide this area into three sub-regions.

## Tibet and Southwestern region

One common feature clearly seen in all tomographic images (Figures 6 and 7) are the relatively low group velocities in the western part of the study area when compared to those of the eastern part. The Tibetan plateau becomes an outstanding enclosed low group velocity feature for Rayleigh wave starting at 40 seconds (Figure 6b); at this period it extends to the

Pamirs as well as eastern Afghanistan and nothern Pakistan. At 30 seconds (Figure 6a), the low group velocity area includes the western Tarim basin to the northwest and to northeast India and western Yunnan. The protrusion toward station KMI is similar to the shape of the Yunnan-Tibet Plateau in that area (Figure 2). This protrusion is no longer visible for periods longer than 40 seconds. The area of lowest velocity is at its maximum for 40 seconds and it continues to shrink for longer periods, with central Tibet as the core of low group velocity. In Bourjot and Romanowicz's (1992) analysis, a similar velocity minimum is seen to persist up to 60 seconds; in our results we see it clearly even at 70 seconds (Figure 6e), albeit the area is smaller. Southern Tibet and the Himalayas are areas of high velocity gradient, so are the northern and eastern edge of the Plateau. The northwestern part of India, where the resolution is good, appears as a high group velocity region.

For Love wave tomography (Figs 7a-e), Tibet emerges as a recognizable low group velocity feature for periods at 40 seconds. At this period, the western Tarim, Pamirs and the Afghanistan-Pakistan low that dominates the tomographic image at 30 seconds is still clear. The Tibet low, however, becomes the dominating feature at 60 and 70 seconds, with the overall shapes significantly different from that for Rayleigh waves. But the Himalayas still appear as a higher gradient zone and northwest India as a relatively high velocity zone.

## Northwestern region

Although the Tarim basin is a major topographic and geological entity, the tomographic image does not show it as a distinctive unit. Southwest Tarim is a region of low group velocity and forms a part of the Tibet low group velocity anomaly for Rayleigh waves at 40, 50 and 60 seconds (Figures 6b-d). Otherwise, Tarim is generally in the transition zone from the low group velocity region of Tibet to the relatively high velocity region to the north. Western Tarim, however consistently shows up as a low velocity unit in the Love wave images at all periods (Figure 7a-e). The Siberian Shield in the northwestern corner of the study area is not a well resolved region in this study; Figures 6c-e do show it as an area of relatively high velocity.

10

As we mentioned earlier, Tienshan is shown to continue from CIS Central Asia to the northern edge of the Tarim Basin (Figure 1) on many tectonic maps (Terman, 1973). But Figures 6a-d and 7a-e show that the group velocities of Rayleigh and Love waves in the section of Tienshan east of LNTS (see figures) is relatively high. Its possible significance will be discussed later.

## Eastern region

Longitude $105°E$ is used as the demarcation for the eastern and western regions of this study. A sharp group velocity transition exists near this longitude, especially in the southern part (Figure 6 and 7).

In the eastern region, Southeastern China is a relatively high group velocity region at all periods. The North China Plain (Figures 1, 6 and 7), on the other hand, appears as a region with medium velocity at 30 seconds for both Rayleigh and Love waves, but becomes a high velocity region at longer periods. Off-shore the Ryukyu backarc basin area has relatively low velocity at all periods studied, but the Japan Sea area is shown as a high velocity region at 30 and 50 seconds for Rayleigh waves and a low velocity area for other periods.

## Tomographic results for $20°N$ to $70°N$ and $40°E$ to $140°E$

In this study we combine data from the study above and data collected by Prof. Anatoli Levshin and K from stations in the former Soviet Union. Although the images in the overlapping area do not differ too much from those contained in Figures 6 and 7, the additional information in Figure 8a-e. We shall only point out a few key features.

## Lake Baikal and Mongolia

Western and eastern Mongolia is separated by a ridge of high velocity that show up in all the images shown in Figures 8a-e. It is especially clear for T = 40, 50 and 60. This ridge coincides generally with the relative Bouguer gravity high extending from Lake Baikal to central Mongolia. There is no clear expression in the surface geology in Mongolia, south of Lake Baikal for this feature. As shown in Figures 8b-d this high velocity ridge is surrounded

11

on the east and west by two low velocity prongs. The nature of this rather major feature is most curious and it could potentially have important influence on reginal wave propagation through this area.

## Siberian platform

The Central and the Western Siberian platforms (Rodriguez, 1969) are, in general, a region of high velocity, especially at longer periods (>50 seconds) as shown in Figures 8c-8e. The relatively thin crust of the central part of this platform and the high upper mantle velocity under the platform is probably responsible for the well defined high velocity region at 70 seconds (Figure 8 e).

## Discussion

The first order tomographic images presented in this paper provide us synoptic views of the lateral variability of the crust and upper mantle in East Asia. Many of the main tectonic units (Figure 1) and topographic features (Figure 2) can be distinguished quite well. Although we prefer not to make further assumptions, which are necessary for the derivation of the dispersion curves and then the velocity structures of various regions from the tomographic results, our maps do provide some quantitative measure of the deep crustal and upper mantle structures under these major features.

The Tibet-Pamir group velocity low dominates the tomographic images at periods greater than 40 seconds (Figures 6b-e). In case of a continental crust, such as that represented by the CANSD model (Brune and Dorman, 1963), Love and Rayleigh waves at 40 seconds or longer have much of their energy traveling in the upper mantle, and therefore sampling that part of the mantle quite well. But for a 70 km Tibetan crust (see Molnar, 1988, for wa summary), Love and Rayleigh waves at 40 seconds are trapped mostly in the crust (Figure 9). These contrasts in eigenfunctions are more pronounced at 70 seconds; at this period the Tibetan-Pamir low is still reflecting the thick low velocity crust, the relatively high velocities in eastern part of China result from thinner crust.

12

Judging from the distribution of group velocities in the Tibet-Pamir area, the crustal thickness is most probably greatest in the central part of Tibet. At 40 seconds, the area of lowest Rayleigh group velocities includes the Kunlun Terrane, the Qiangtang Terrane as well as a part of the Lhasa Terrane north of the Himalayas (Dewey et al., 1988). As noticed by Bourjot and Romanowicz (1992), the Tibetan low velocity feature clearly extends to the southwestern part of the Tarim Basin (see Figures 2 and 6b-c), where a basin with thick (>8 km) sediments exists (Terman, 1973). For Love waves, at 40 and 50 seconds (Figures 7b-c) the low velocity in Tibet is not as pronounced as that in Pamir, but the low velocity area is very prominent at 60 and 70 seconds (Figures 7d and 7e). The low velocity area extends to southwest Tarim also. The low velocity area in both cases is surrounded by areas with high group velocity gradients. Tarim basin as a whole is in the gradient zone.

We have noted earlier that the Tienshan fold belt as east of longitude 87°E (Figure 1) is noticeably distinct from the western part in that whereas the western part reveals itself as an area with low Rayleigh wave group velocity, the eastern part is an area of relatively high velocity. This feature seems to be consistent with the observation that the Bouguer gravity low (Figure 3) associated with western Tienshan (the -250 mgal contour) terminates there. Also, as noted earlier, the Tienshan here is actually a E-W striking basin and range province, with the presence of the sub-sea level Turfan basin as the lowest point. Evidently, this is a deep-seated feature, with a thin crust underneath, resulting perhaps from north-south tension. The seismicity of western section of Tienshan is rather high with large thrust events; in contrast eastern Tienshan is not very seismic.

The increase in group velocities of both the Rayleigh and Love waves eastward across 105°E is clear in Figures 6b-e and 7b-e. The trend agrees generally with that shown in the Bouguer gravity map (Figure 3). In the eastern half of the study area, the relatively high velocity region south and east of Beijing (the North China Plain) is easily distinguished; it is evidently related to the thin crust in that region, with thicknesses generally less than 35 km (Wang and Mao, 1985); the high group velocity here reflect the upper mantle structures. The North China Plain is a region of active extensional tectonics (Nabelek et. al., 1987) where many large earth-

quakes were located. Southeastern China is also a region of relatively high velocities especially at periods less than 70 seconds. Here the thin crust (~32 km) is probably the main controlling factor. In contrast to North China Plain, this region is not tectonically active. The Japan Sea area appears as a high velocity region for Love and Rayleigh waves at 40 seconds (Figures 6b and 7b), but becomes an area of relatively low velocity for longer period Rayleigh waves (e.g., Figure 6d and 6e).

The interpretation of the new images made with combined datasets is not yet complete. One of the obvious and very significant feature observed in the images is the high velocity ridge extending from Lake Baikal southward through Mongolia. The nature of this ridge is to be investigated further. In view of the fact that Lake Baikal is a young and active tectonic unit, this southern extension may indicate a continuation of the rifting. Having started only recently, it has not yet had generated any surface expresion. Further studies are made possible with the recent establishment of the IRIS/Soviet network.

## Conclusion

The results of this surface wave tomographic inversion study provides clear images of the variable nature of the deep crustal and upper mantle structures under eastern Asia as a whole. The surface wave tomographic technique is evidently a powerful one for this area where a few high quality digital seismic stations exist and where there are a large number of moderate to strong earthquakes in and around the study area. To further refine the group velocity maps, it is necessary to consider curved wave paths in future work since the velocity gradients we see in these images are quite high, with total group velocity changes on the order of $\pm 15\%$ in the study area.

## Acknowledgement

14

assisted ably; we would like to mention especially D. Salzberg, Y. L. Kung and R. J. Rau. We also thank Bob Hutt of Albuquerque Seismic Laboratory (ASL), USGS for giving us a copy of his instrument response program.

# References

Backus, G. and Gilbert, F., 1968. The resolving power of gross Earth data. Geoph. J. Roy. Astr. Soc., 16: 169-205.

Backus, G. and Gilbert, F., 1970. Uniqueness in the inversion of innacurate gross Earth data. Phil. Trans. Roy. Soc. London, 226: 123-192.

Bourjot, L. and Romanowicz, B., 1992. Crust and upper mantle tomography in Tibet using surface waves. Geophys. Res. Lett., 19: 881-884.

Brandon, C. and Romanowicz, B., 1986. A "no-lid" zone in the central Chang-Thang platform of Tibet: Evidence from pure path phase velocity measurements of long period Rayleigh waves. J. Geophys. Res., 91: 6547-6564.

Brune, J.N. and Dorman, J., 1963. Seismic waves and Earth structure in the Canadian Shield. Bull. Seism. Soc. Am., 53: 167-509.

Chen, W.P. and Molnar, P.,1981. Constraints on the seismic wave velocity structure beneath the Tibetan plateau and their tectonic implications. J. Geophys. Res., 86: 5937-5962.

Chun, K. Y. and McEvilly, T. V., Crustal structure in Tibet: High seismic velocity in the lower crust, J. Geophys. Res., **91**, 10405-10411, 1986.

Chun, K. Y. and Yoshii, T., Crustal structure of the Tibetan Plateau: A surface wave study by a moving window analysis, Bull. Seismo. Soc. Am., **67**, 737-750, 1977.

Dewey, J.F., F.R.S., Shackeleton, R.M.,F.R.S., Chang C.F., and Sun Y.Y., 1988. The tectonic evolution of the Tibetan Plateau, Phil. Trans. Roy. Soc. London. A 327: 379-413.

Ditmar, P.G. and Yanovskaya, T.B., 1987. A generalization of the Backus-Gilbert method for estimation of lateral variations of surface wave velocity. Izv. AN SSSR, Fizika Zemli (Solid Earth), no. 6: 30-60.

Feng, C. C. and Teng, T., 1983. Three-dimensional crust and upper mantle structure of the Eurasian continent. J. Geophys. Res., 88: 2261-2272.

Feng, R., Zhu, J.S., Ding, Y.Y., Chen, G.Y., He, Z.Q., Yang, S.B., Zhou, H.N. and Sun, K.Z., 1983. Crustal structure in China from surface waves. Chinese Geophysics, Am. Geophys. Union, 2: 273-289.

Rodriguez, R.G., 1969. Atlas of Asia and eastern Europe, Volume V. Crust and Upper Mantle, USGS.

Gupta, H.K., and Narain, H., 1967. Crustal structure of the Himalayan and Tibet Plateau from surface wave dispersion. Bull. Seismo. Soc. Am., 57: 235-248.

Hirn, A., 1988. Features of the crust-mantle structure of Himalayas-Tibet: a comparison with seismic traverses of Alpine, Pyrenean and Variscan orogenic belts. Phil. Trans. Roy. Soc. London. A 327: 17-32.

Jobert, N. and Jobert, G., 1983. An application of the ray theory to the propagation of waves along a laterally heterogeneous spherical surface. Geoph. Res. Lett., 10: 1148-1151.

Kozhevnikov, V.M. and Barmin, M.P., 1989. Dispersion curves of Rayleigh wave group velocities for several regions of the Asian continent. Izv. AN SSSR, Fizika Zemli (Solid Earth), no. 9: 16-25.

Kozhevnikov, V.M., Lokshtanov, D.E. and Barmin, M.P., 1992. Shear-velocity structure of the lithosphere for nine large tectonic regions of the Asian continent. Izv. AN SSSR, Fizika Zemli (Solid Earth), no. 1: 61-70.

Levshin, A. L., F. T. Wu, and V. M. Kozhevnikov, 1993. Surface wave tomography of eastern Asia, to be presented at Spring 1993, AGU in Baltimore.

Levshin, A.L., Yanovskaya, T.B., et al., 1989. Seismic Surface Waves in a Laterally Inhomogeneous Earth. Editor Keilis-Borok, V.I., Kluwer Acad. Publ., Dordrecht/ Boston/ London.

McCowan, D.W. and Lacoss, R.T., 1978. Transfer functions for the Seismic Research Observatory seismograph systems. Bull. Seism. Soc. Am., 68: 501-512.

Molnar, P., 1988, A review of geophysical constraints on the deep structure of the Tibetan Plateau, the Himalaya and the Karakoram and their tectonic implications. Phil. Trans. Roy. Soc. London. A 327: 33-88.

Molnar, P., and Lyon-Caen, H., 1989. Fault plane solutions of earthquakes and active tectonics of the Tibetan Plateau and its margins, Geophys. J. Int., 99: 123-153.

Molnar, P. and Tapponnier, P., Active tectonics of Tibet, J. Geophys. Res., 83: 5361-5375.

Nabelek, J., Chen, W.P., and Ye, H., 1987. The Tangshan earthquake sequence and its implications for the evolution of the North China Basin. J. Geophys. Res., 92: 12615-12628.

Patton, H., 1980. Crustal and upper mantle structure of the Eurasian continent from the phase velocity and Q of surface waves. J. Rev. Geophys. Space Phys. 18: 605-625.

Pines, I., Teng, T., Rosenthal, R. and Alexander, S., 1980. A surface wave dispersion study of the crustal and upper mantle structure of China. J. Geophys. Res., 85: 3829-3844.

Terman, M., 1973. Tectonic Map of China and Mongolia. Geol. Soc. of Am., Boulder, Colorado.

Tikhonov, A.N. and Arsenine,V., 1976. Methodes de resolution de problemes mal poses. MIR Publishers, Moscow.

USAF, 1971. Bouguer gravity anomaly map of Asia. Aeronautical Chart and Information Center, St. Louis, Mo., USA.

Wang, G.Z., and Mao, E.T., (Eds.) 1985. Crust and Upper Mantle in China, Results of Geophysical Exploration. Seismological Press, Beijing, China.

Wier, S. 1983. Surface wave dispersion and Earth structure in South-Eastern China. Geophys. J. Roy. Astr. Soc., 89: 33-47.

Wu, F. T. and A. L. Levshin, 1993. Surface wave group velocity tomography of east Asia, submitted to special GEOSCOPE issue of Physics of the Earth and Planetary Interior, Feb. 1993.

Yang, T. Y., Chen, Y. Q., and Wang, H. Z., 1986. The Geology of China, Oxford Monograph, no. 3, 303p.

Yanovskaya, T.B., 1982. Distribution of surface wave group velocities in the North Atlantic. Izv. AN SSSR, Fizika Zemli (Solid Earth), no. 2: 3-11.

Yanovskaya, T.B. and Ditmar, P.G., 1990. Smoothness criteria in surface wave tomography. Geophys. J. Int., 102: 63-72.

Zhao L.S., Helmberger, D. and Harkrider, D., 1991. Shear-velocity structure of the crust and upper mantle beneath the Tibetian Plateau and southeastern China. Geoph. J. Int., 105: 713-730.

## Table 1.

Inversion parameter and residuals for different waves and periods for the CDSN/SRC dataset

| Period Sec | Number of paths | Average velocity KM/S | Average residual Sec |
|------------|-----------------|------------------------|----------------------|
| LOVE WAVES | | | |
| 30 | 358 | 3.35 | 27.2 |
| 40 | 357 | 3.52 | 25.7 |
| 50 | 357 | 3.67 | 27.8 |
| 60 | 349 | 3.82 | 32.8 |
| 70 | 344 | 3.93 | 40.1 |
| RAYLEIGH WAVES | | | |
| 30 | 362 | 3.08 | 28.2 |
| 40 | 362 | 3.30 | 23.7 |
| 50 | 362 | 3.48 | 24.0 |
| 60 | 362 | 3.61 | 21.0 |
| 70 | 361 | 3.70 | 21.9 |

## Figures

Figure 1. Generalized tectonic map of Eastern Asia (after Terman, 1973).

Figure 2. Topography of Eastern Asia based on the ETOPO5 topographic database. Locations of stations and some of the events used in the study are shown as triangles and circles respectively. Station CHTO is below latitude 20 at longitude 100 E. Notice that many of the tectonic units shown in Fig. 1 are clearly associated with major topographical features. The Tibetan Plateau is the most prominent feature on this map. The Tarim Basin north of the Tibet where the Lop Nor Test Site (LNTS) is is bounded on the sorth by Tibet and the Tienshan to the north. Although the eastern section of Tienshan southeast of WMQ station is a continuation of the western Tienshan, there is actually a graben with its lowest point in the Turfan Basin (-280m). The Szechuan Basin

(red area north of KMI station) is surrounded by 1000-2000 mountain ranges. The topography of western China is in general much higher than the eastern quarter. The area southeast of BJI station is the North China Plain.

Figure 3. Simplified Bouguer gravity map of the study area (USAF, ).

Figure 4. Instrument group delays for World Wide Standard Seismograph Network (WWSSN), Chinese Digital Seismic Network (CDSN), Seismic Research Observatory (SRO) instruments at TATO (August 28, 1980 to mid-1992) and MAJO (MAJO1 valid for the period August 23, 1988 through August 20, 1990, and MAJO2 valid for August 20, 1990 through February 8, 1991).

Figure 5. Path coverage for this study. Along most of the paths both Love and Rayleigh waves are available. For differnet periods the coverage varies slightly.

Figure 6. Rayleigh wave group velocity tomographic inversion results for (a) 30 seconds, (b) 40 seconds, (c) 50 seconds, (d) 60 seconds, and (e) 70 seconds. (f) Resolution at 50 seconds. Note the different scale for each figure.

Figure 7. Love wave group velocity tomographic inversion results for (a) 30 seconds, (b) 40 seconds, (c) 50 seconds, (d) 60 seconds, and (e) 70 seconds. (f) Resolution at 50 seconds. Note the different scale for each figure.

Figure 8. Rayleigh wave group velocity tomographic inversion results using expanded dataset for (a) 30 seconds, (b) 40 seconds, (c) 50 seconds, (d) 60 seconds, and (e) 70 seconds. Note the different scale for each figure.

Figure 9. Eigenfunctions for Rayleigh (R) and Love (L) waves at 40 and 70 seconds for two extreme models: an approximate Tibet model (T) with a 70 km thick crust, and the Canadian Shield model (C) (Brune et al., 1963). TL = Tibetan Love wave, TR = Tibetan Rayleigh, CL = Shield Love and CR = Canadian Rayleigh. For Rayleigh waves only the vertical (radial) eigenfunctions are shown.
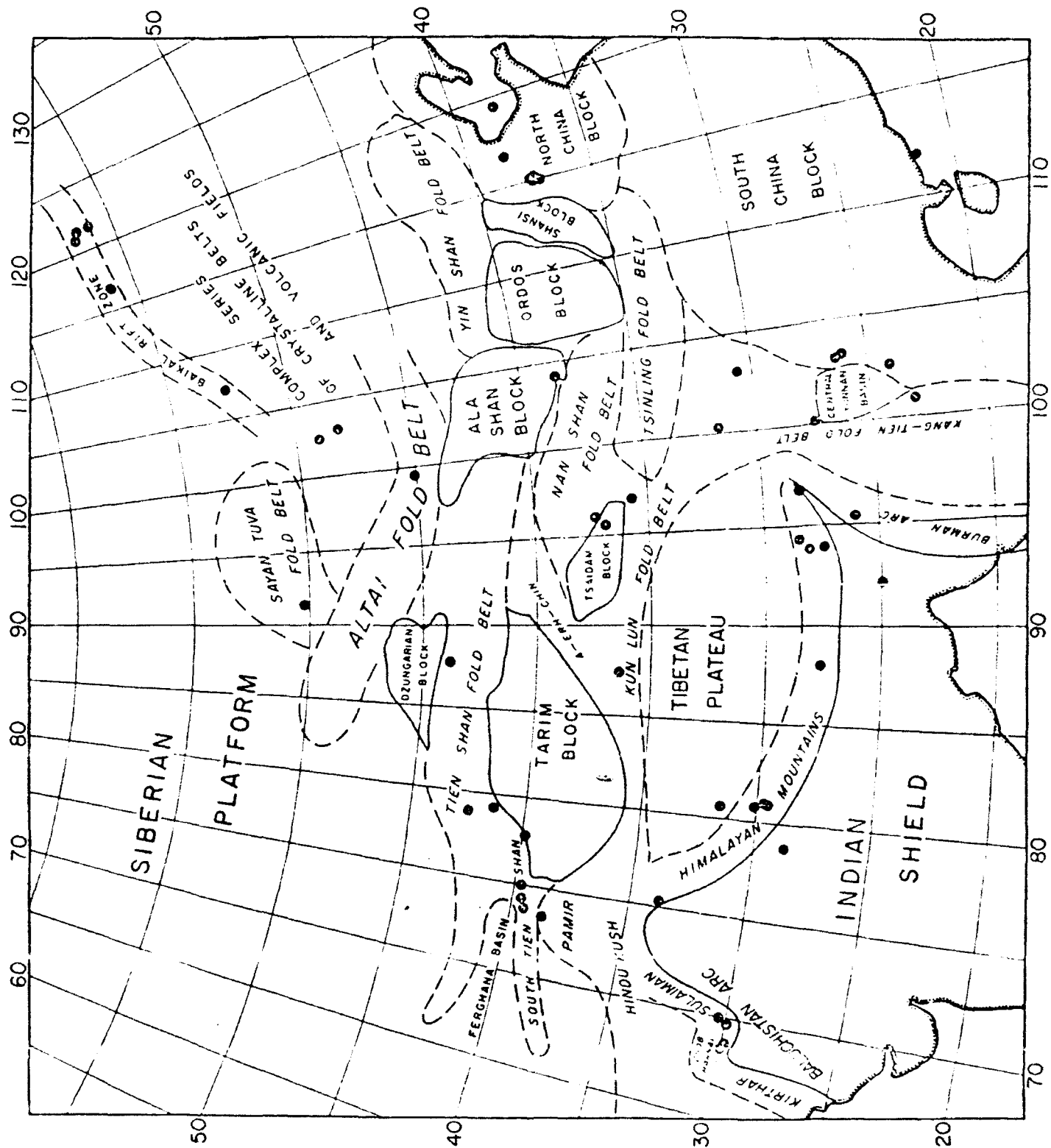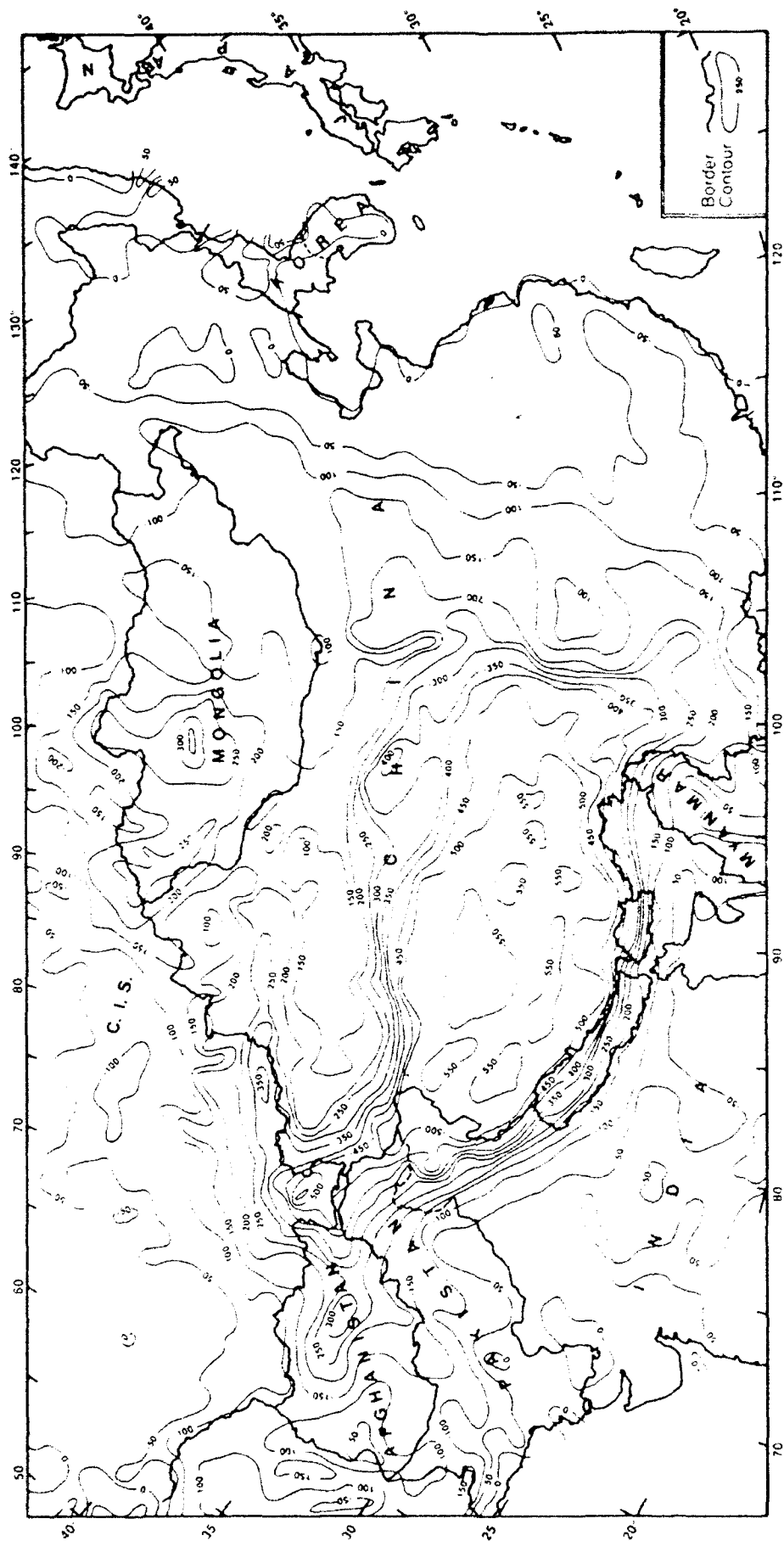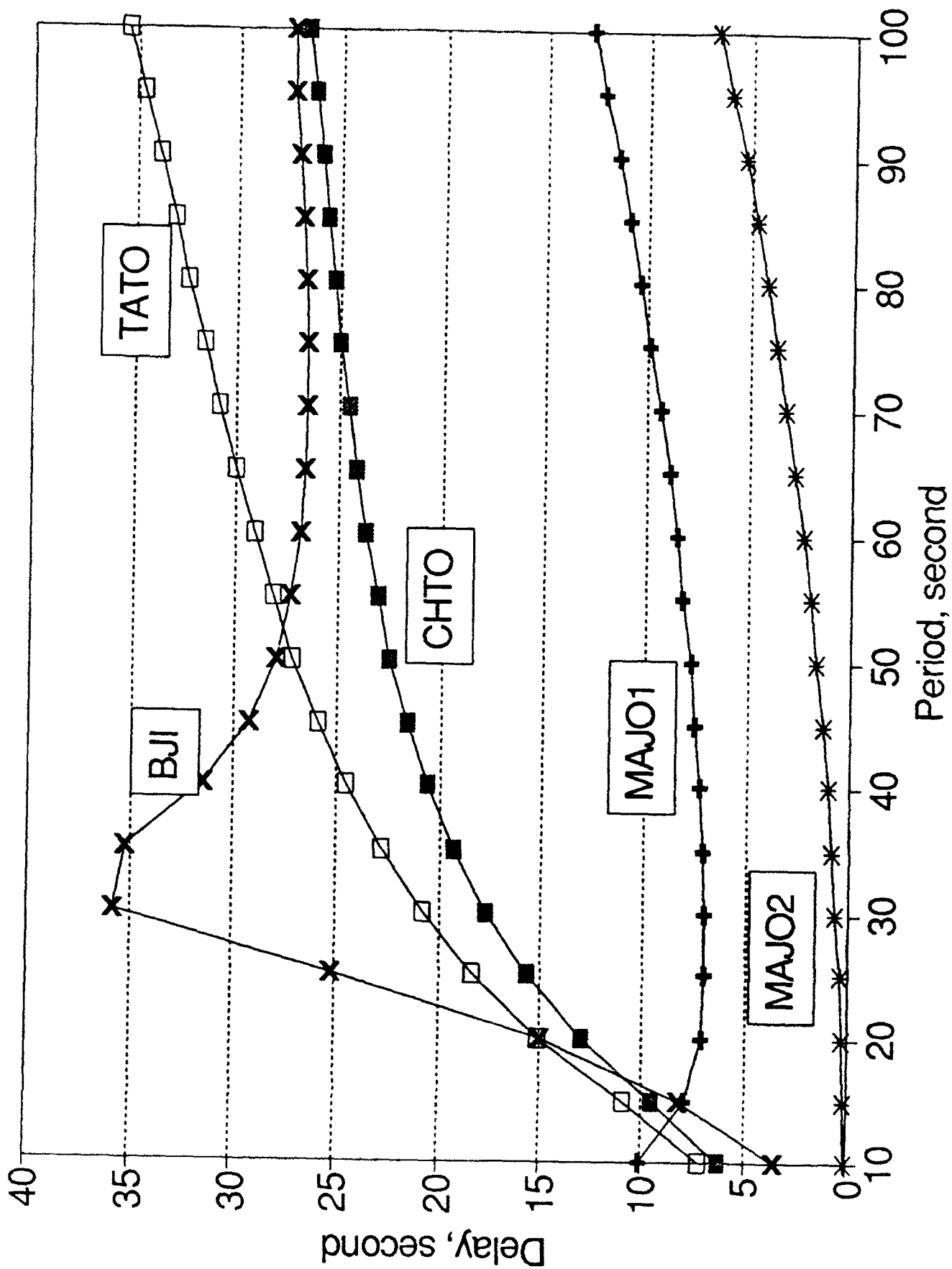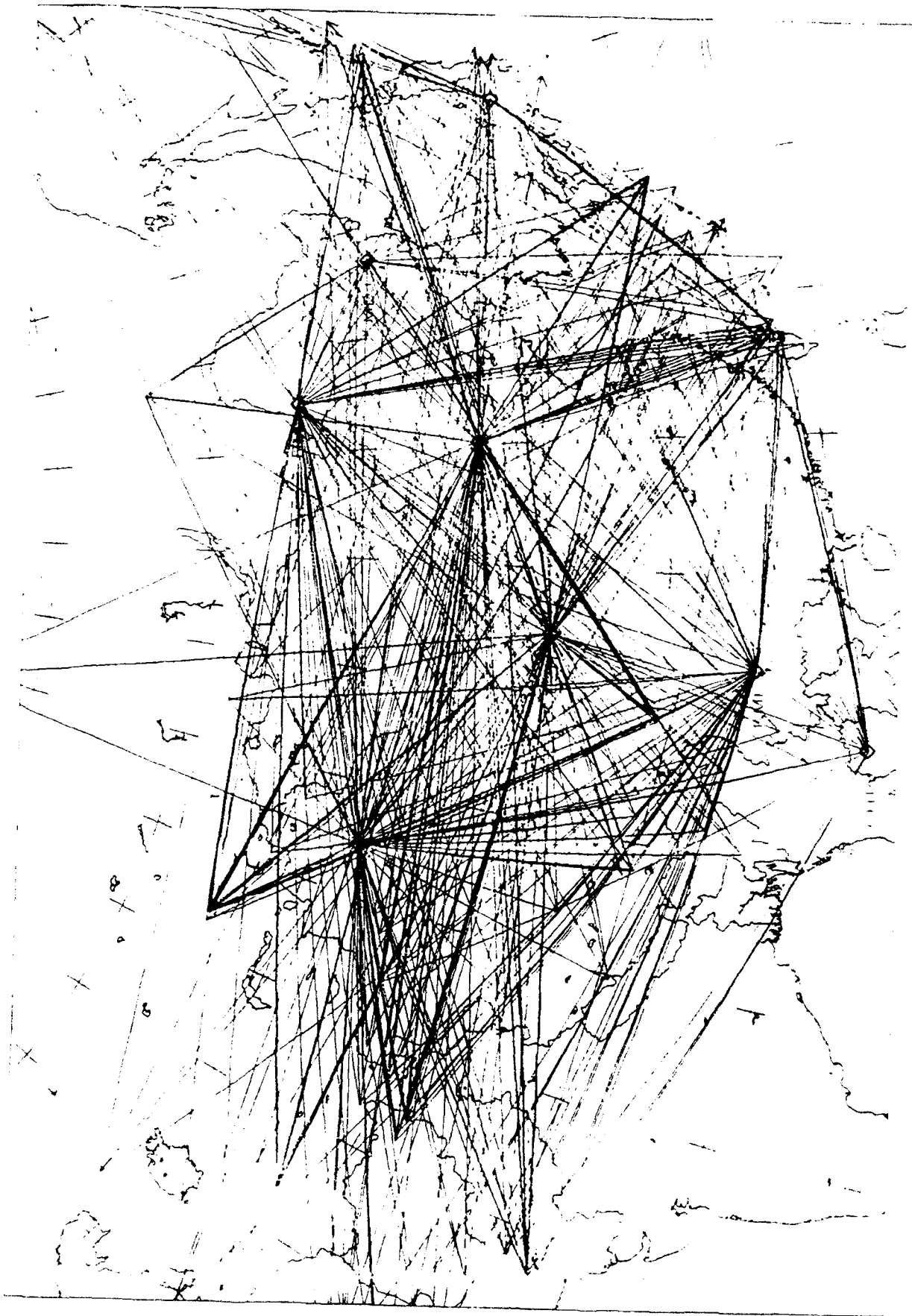
Figure 1
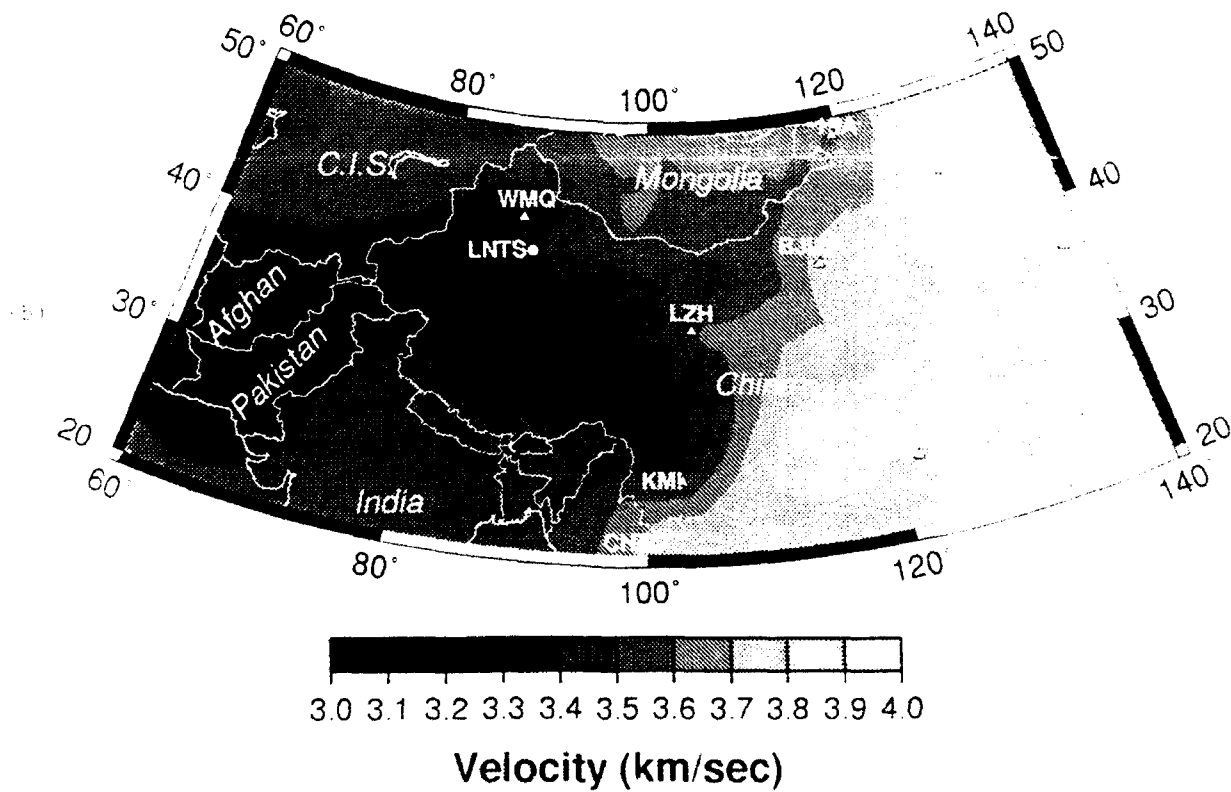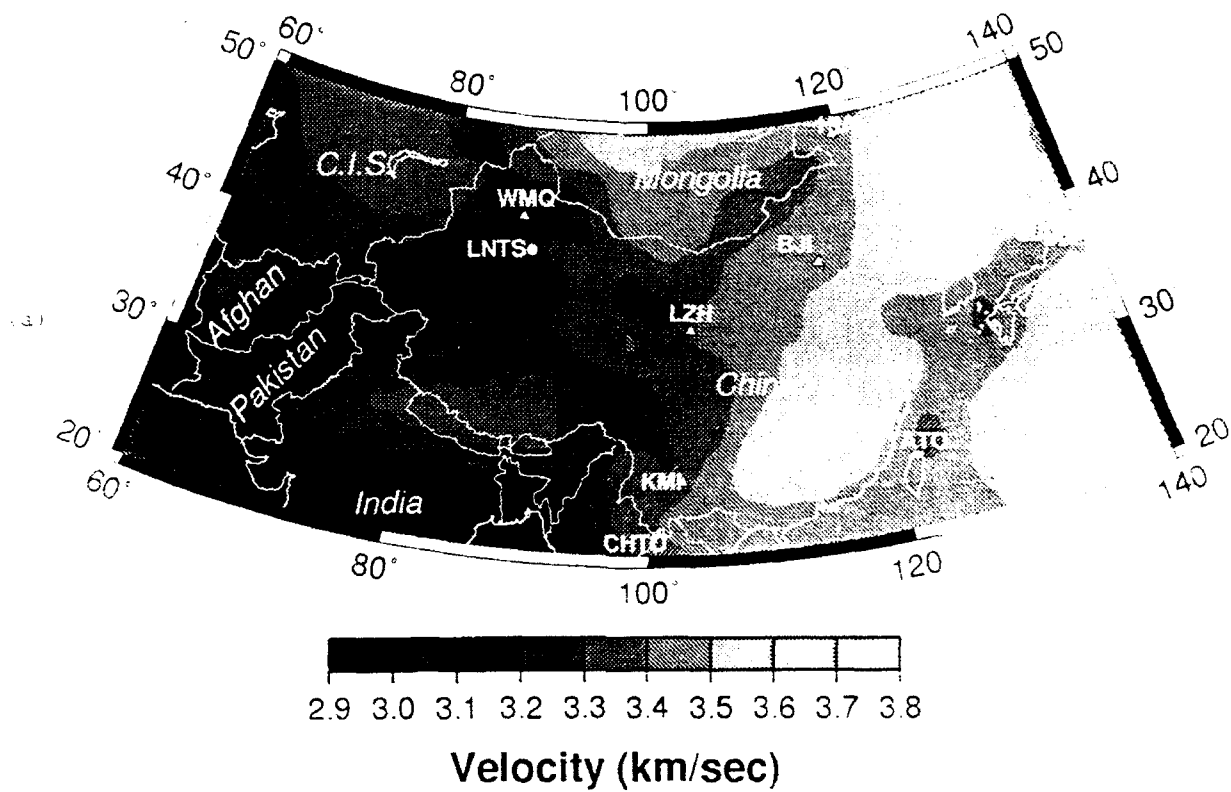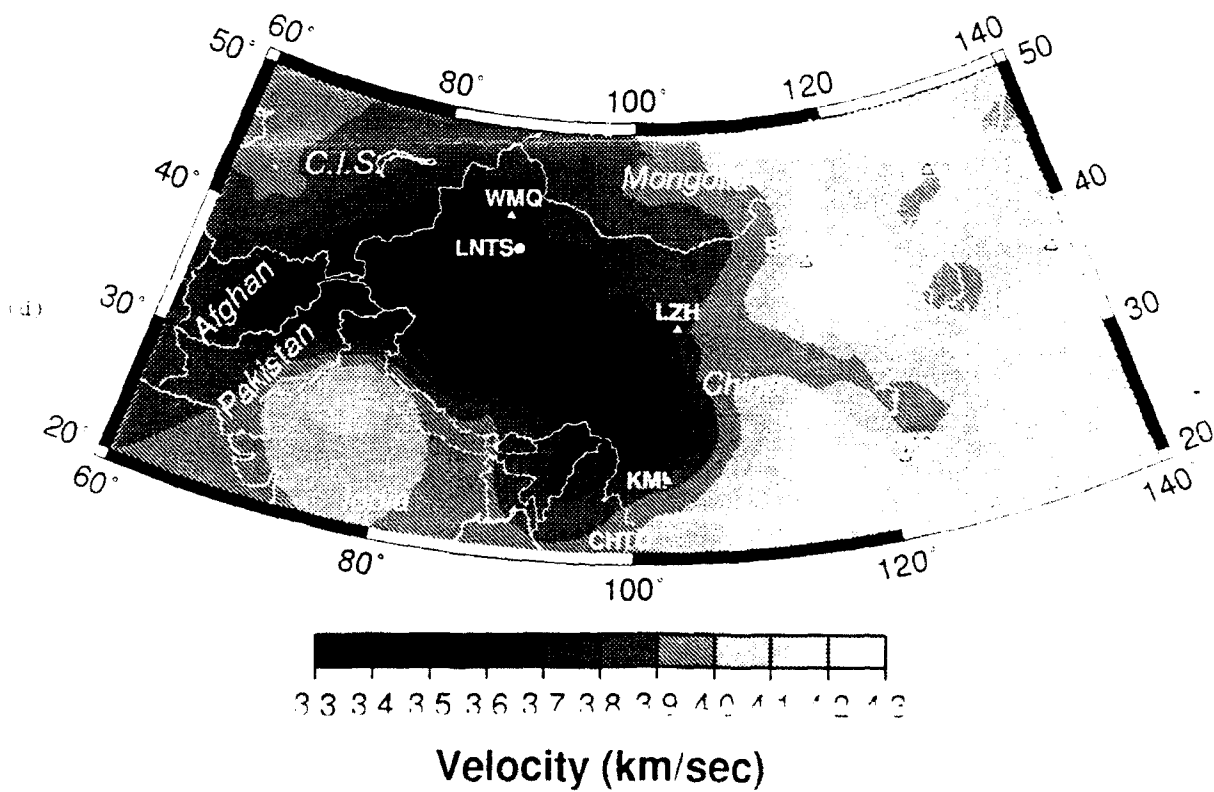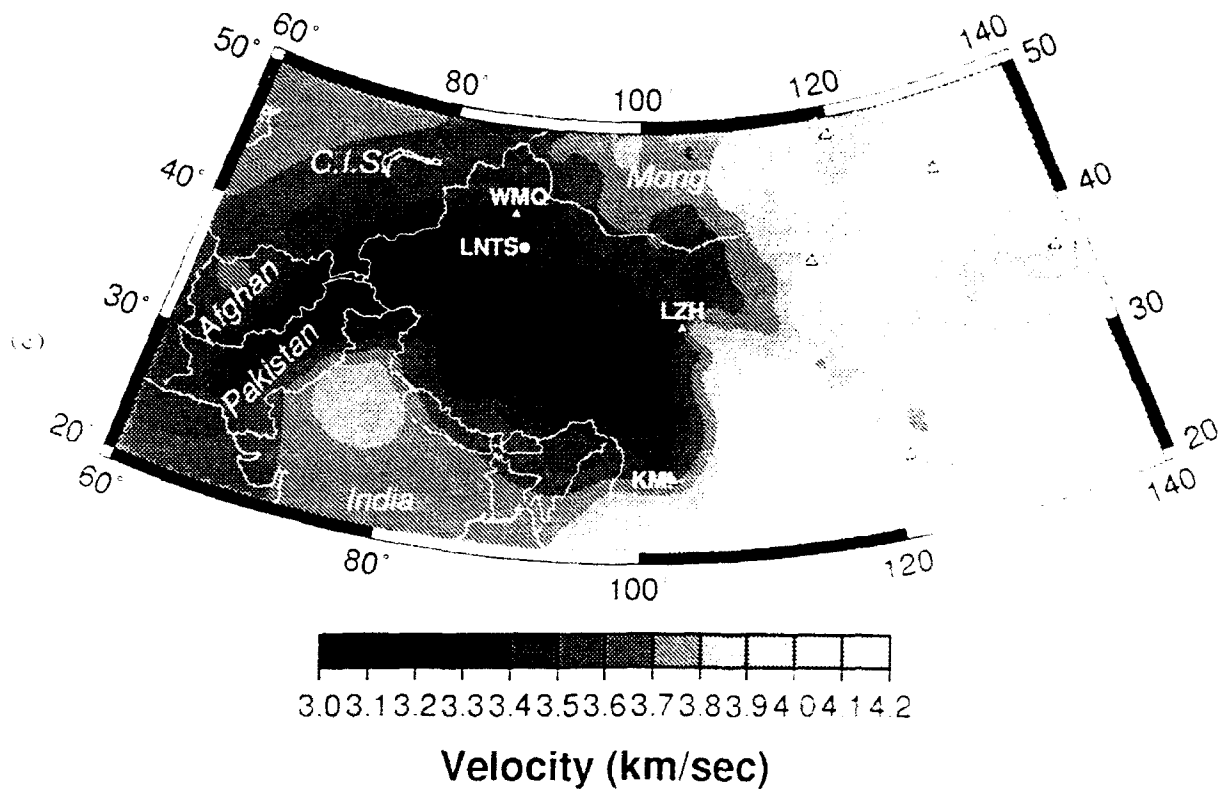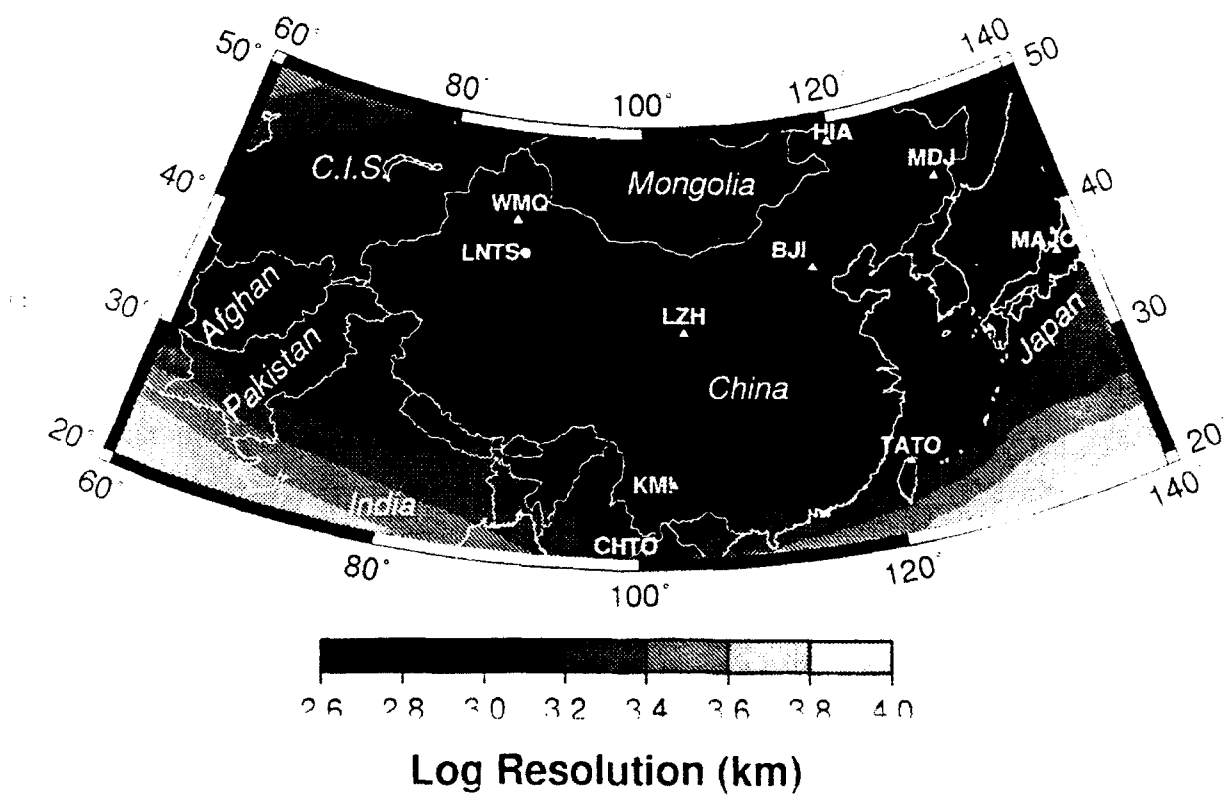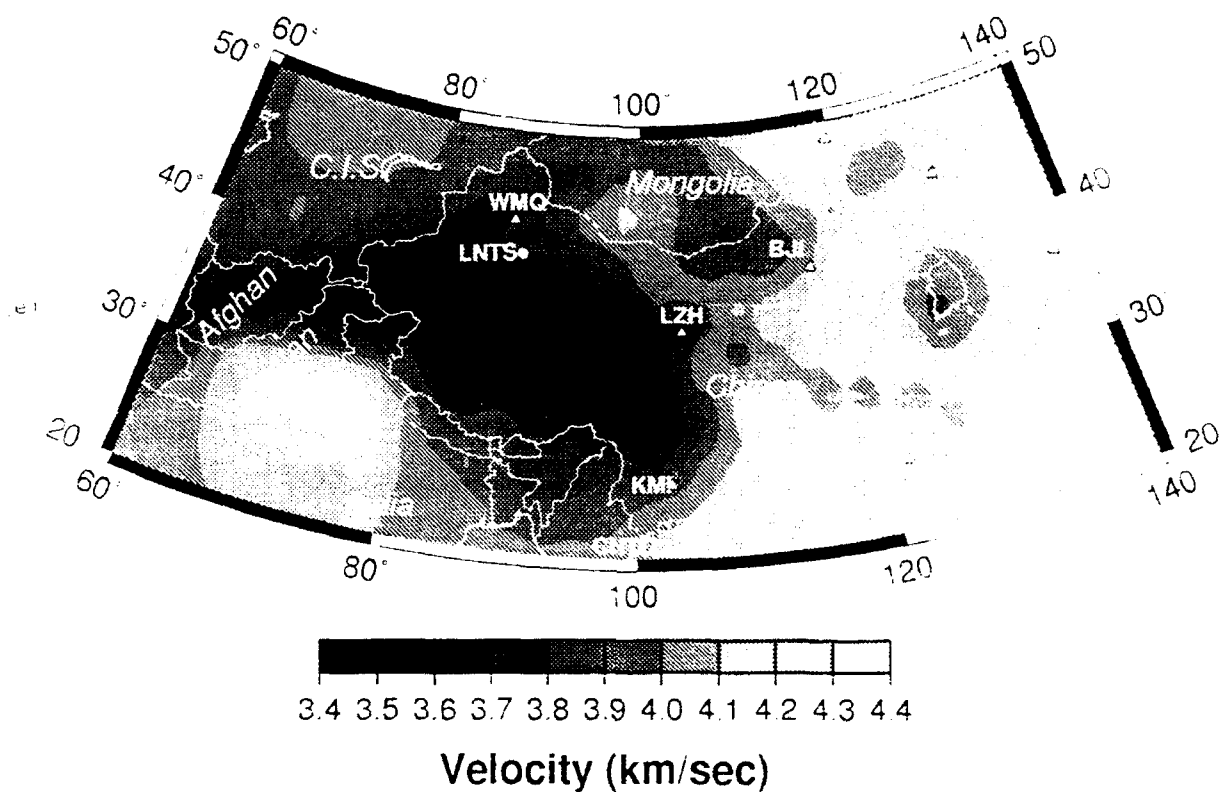
Elevation (meters)

0  500 1000 1500 2000 2500 3000 3500 4000 4500 5000

Figure 3

23

Figure 4

24

Figure 5

25

Velocity (km/sec)



Velocity (km/sec)

Figure 6

26

**Velocity (km/sec)**

3.0 3.1 3.2 3.3 3.4 3.5 3.6 3.7 3.8 3.9 4.0 4.1 4.2



**Velocity (km/sec)**

3.3 3.4 3.5 3.6 3.7 3.8 3.9 4.0 4.1 4.2 4.3

Figure 5

27

Velocity (km/sec)



Log Resolution (km)

Figure 6
28

**Velocity (km/sec)**

2.7 2.8 2.9 3.0 3.1 3.2 3.3 3.4 3.5 3.6



**Velocity (km/sec)**

2.7 2.8 2.9 3.0 3.1 3.2 3.3 3.4 3.5 3.6 3.7 3.8

Figure 7
29

Velocity (km/sec)

Velocity (km/sec)

Figure 7
30

Velocity (km/sec)

3.2  3.3  3.4  3.5  3.6  3.7  3.8  3.9  4.0
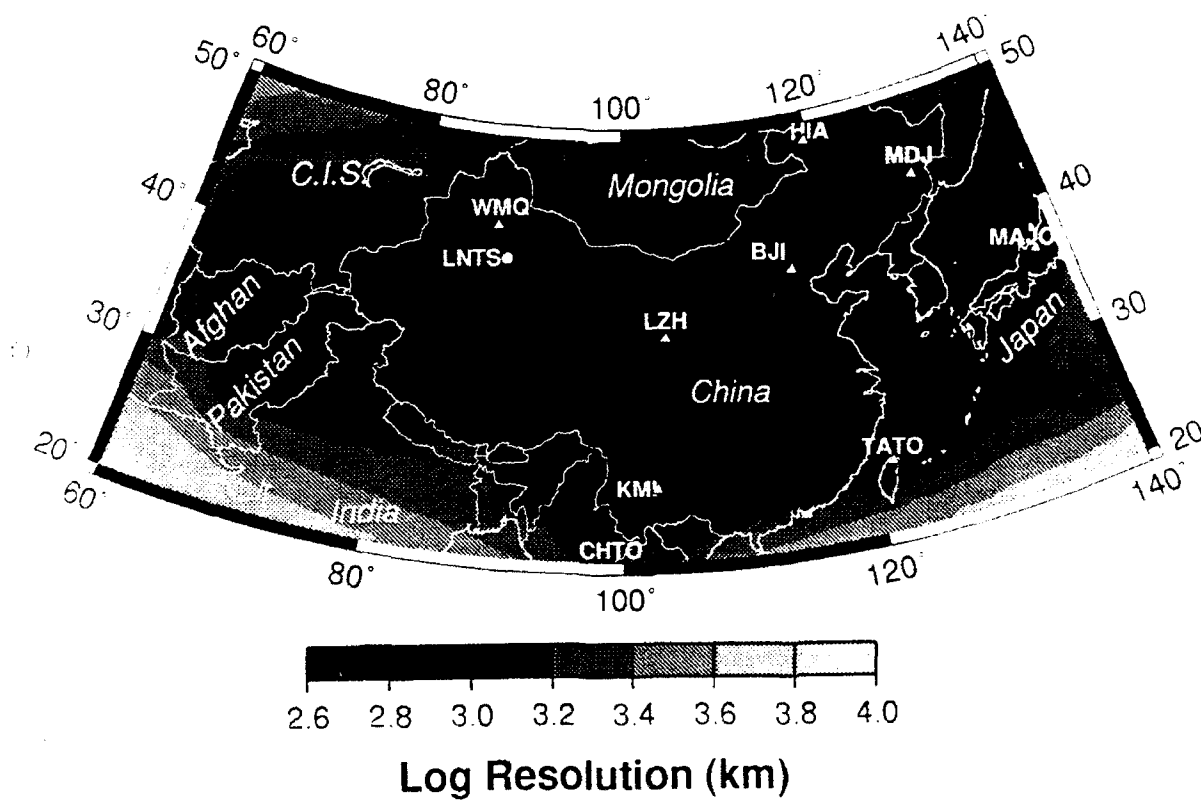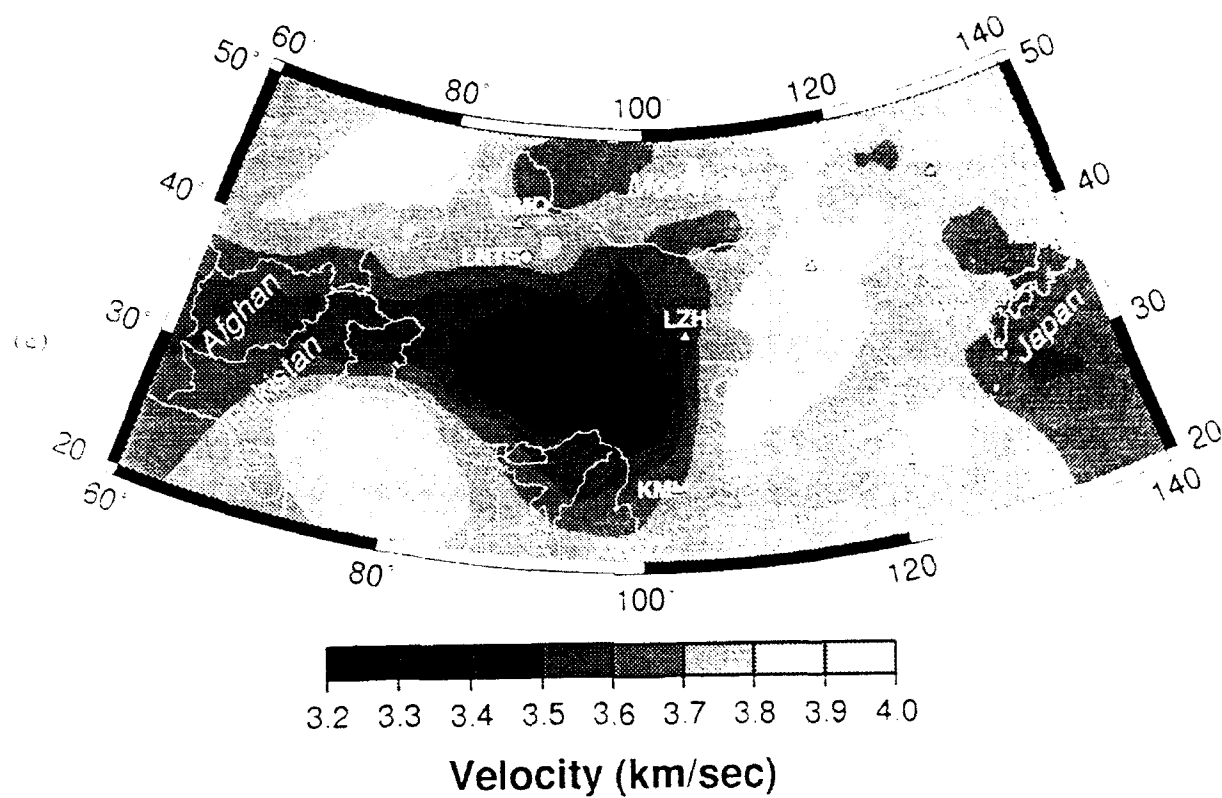


Log Resolution (km)

2.6  2.8  3.0  3.2  3.4  3.6  3.8  4.0
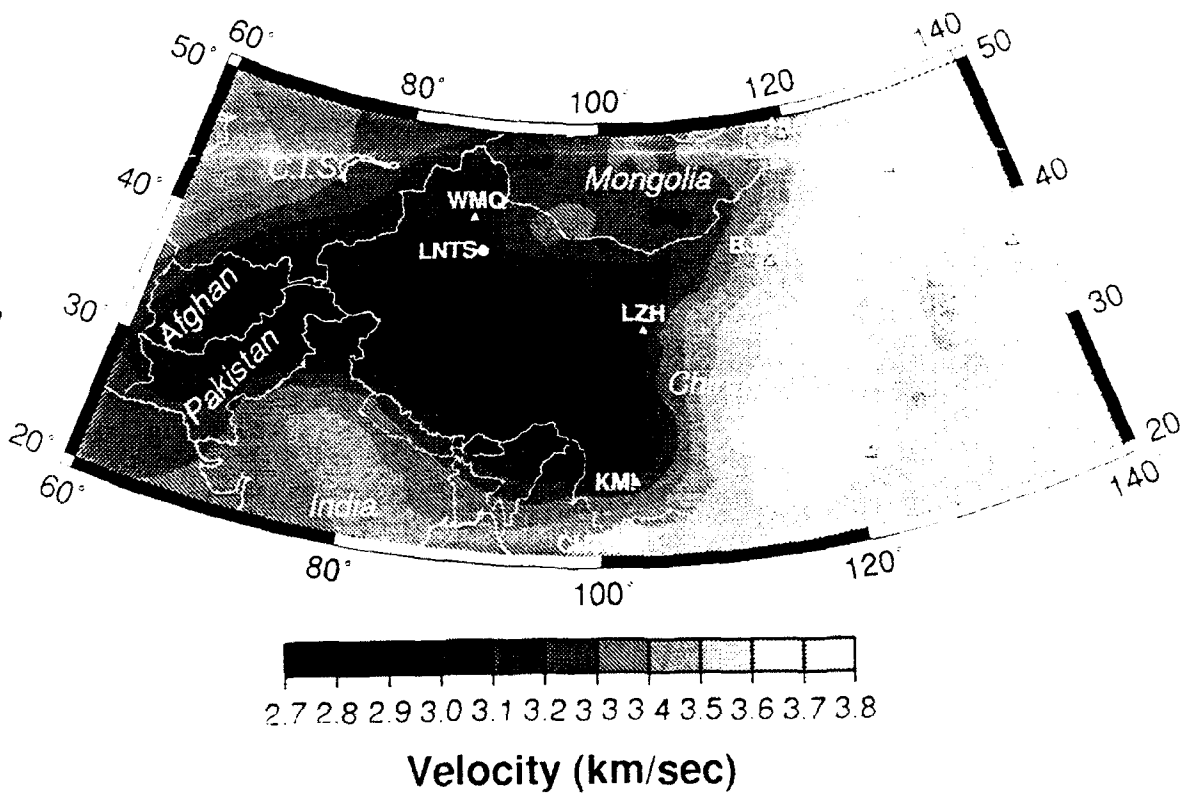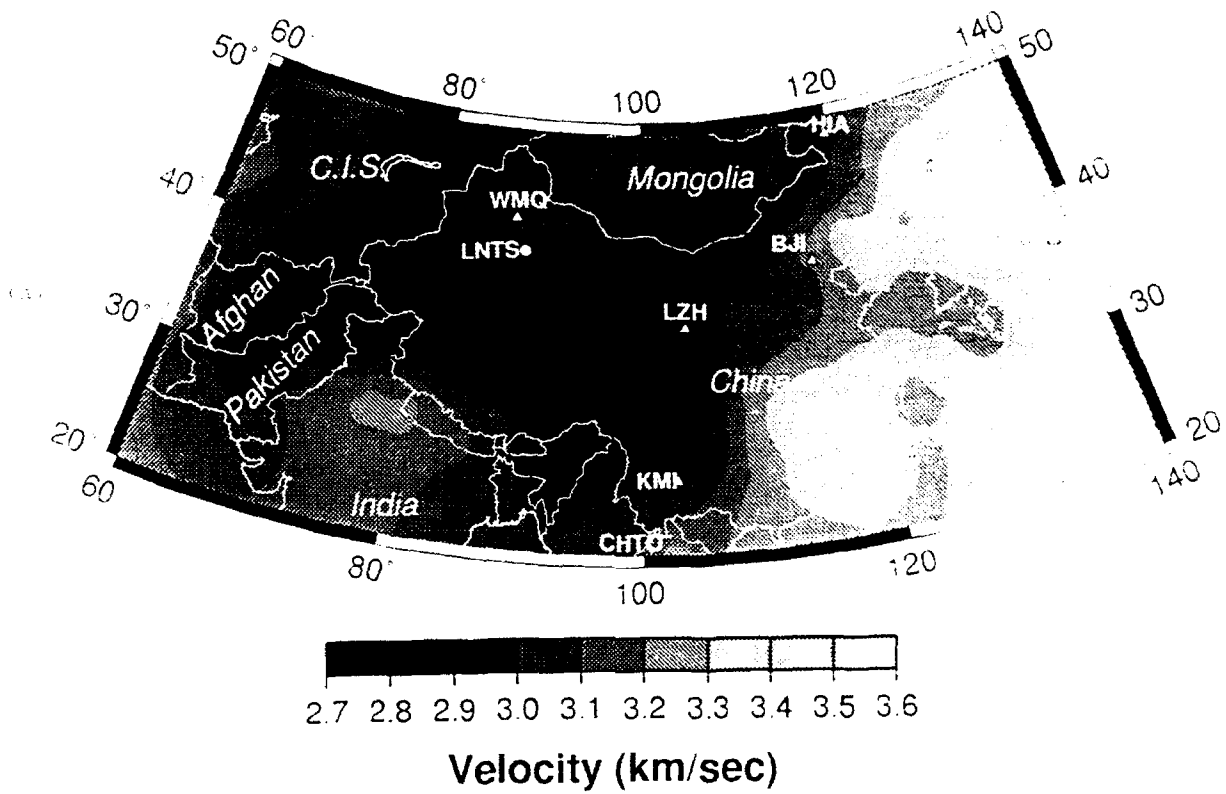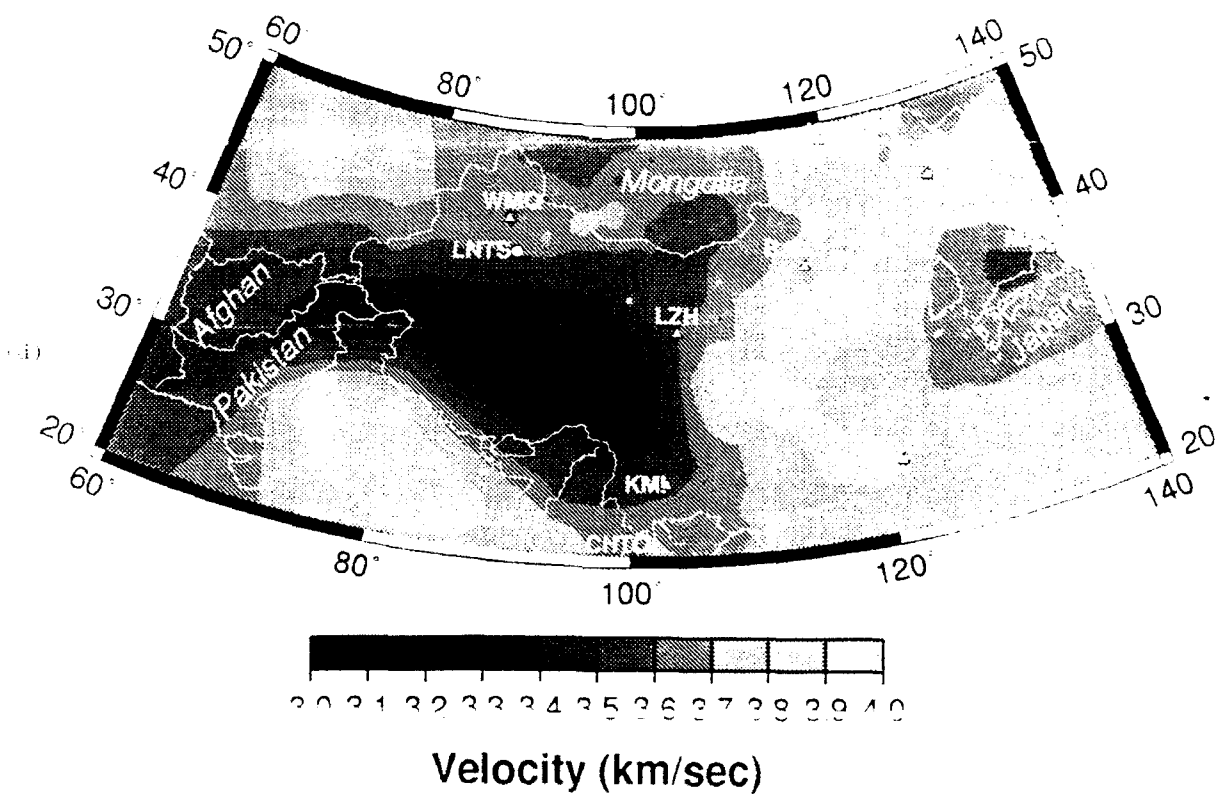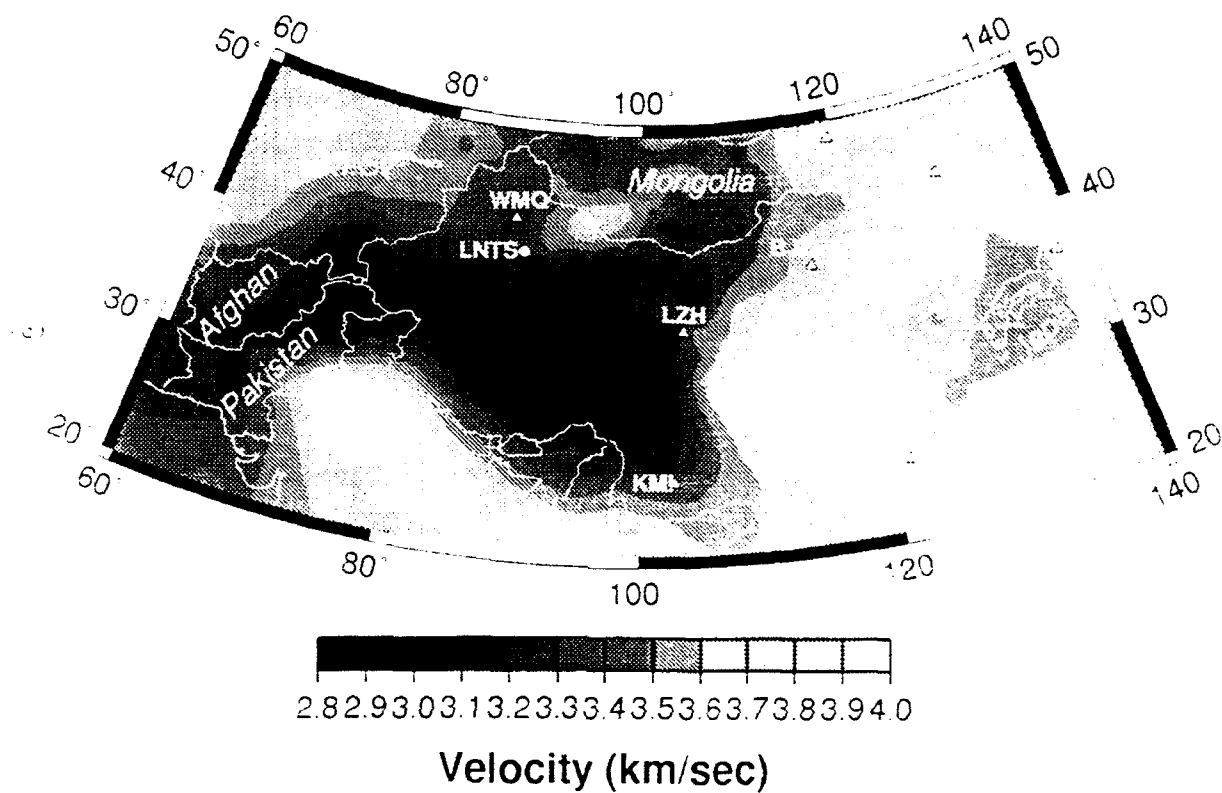
Figure 7
31

Figure 3.1
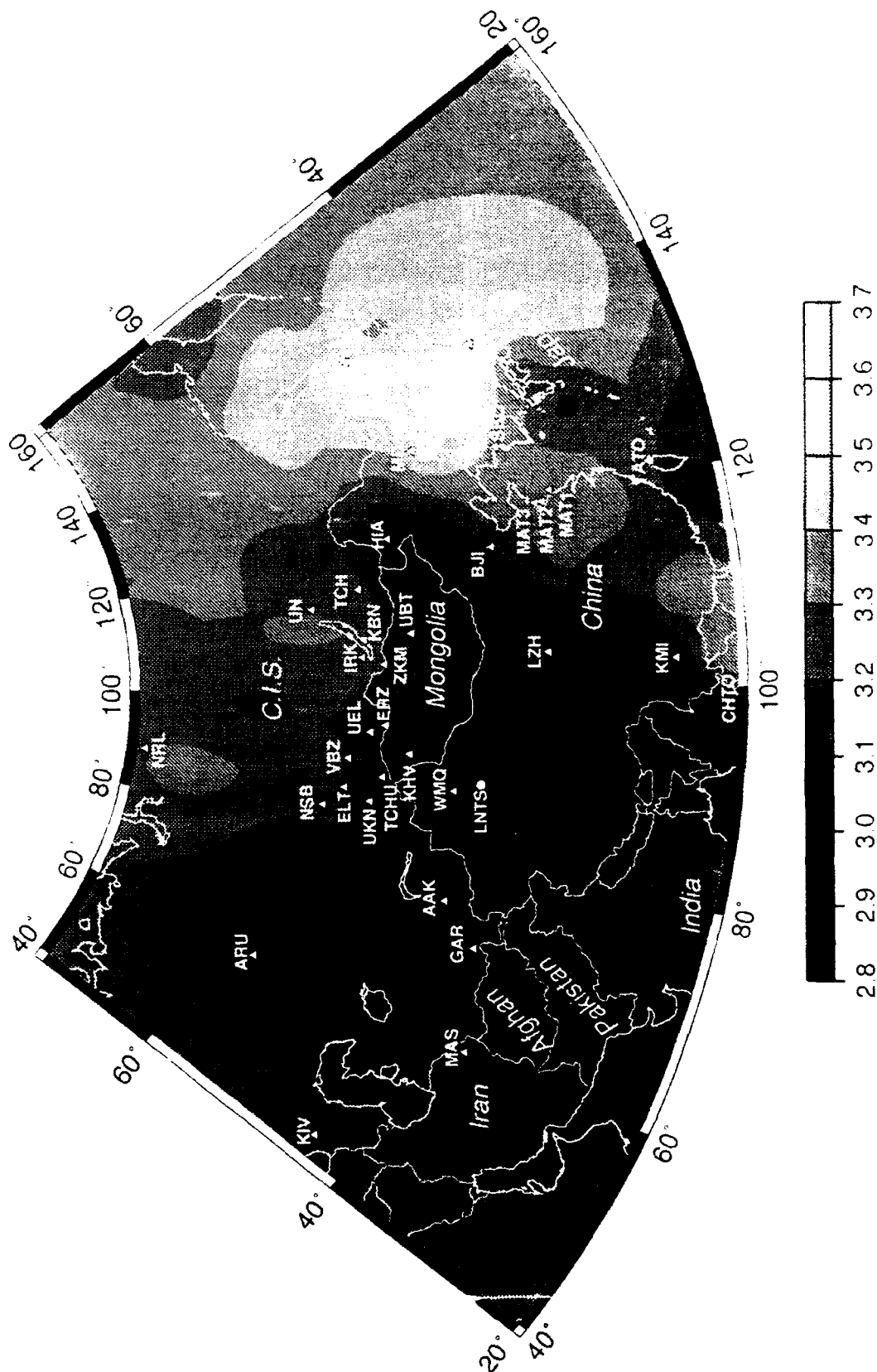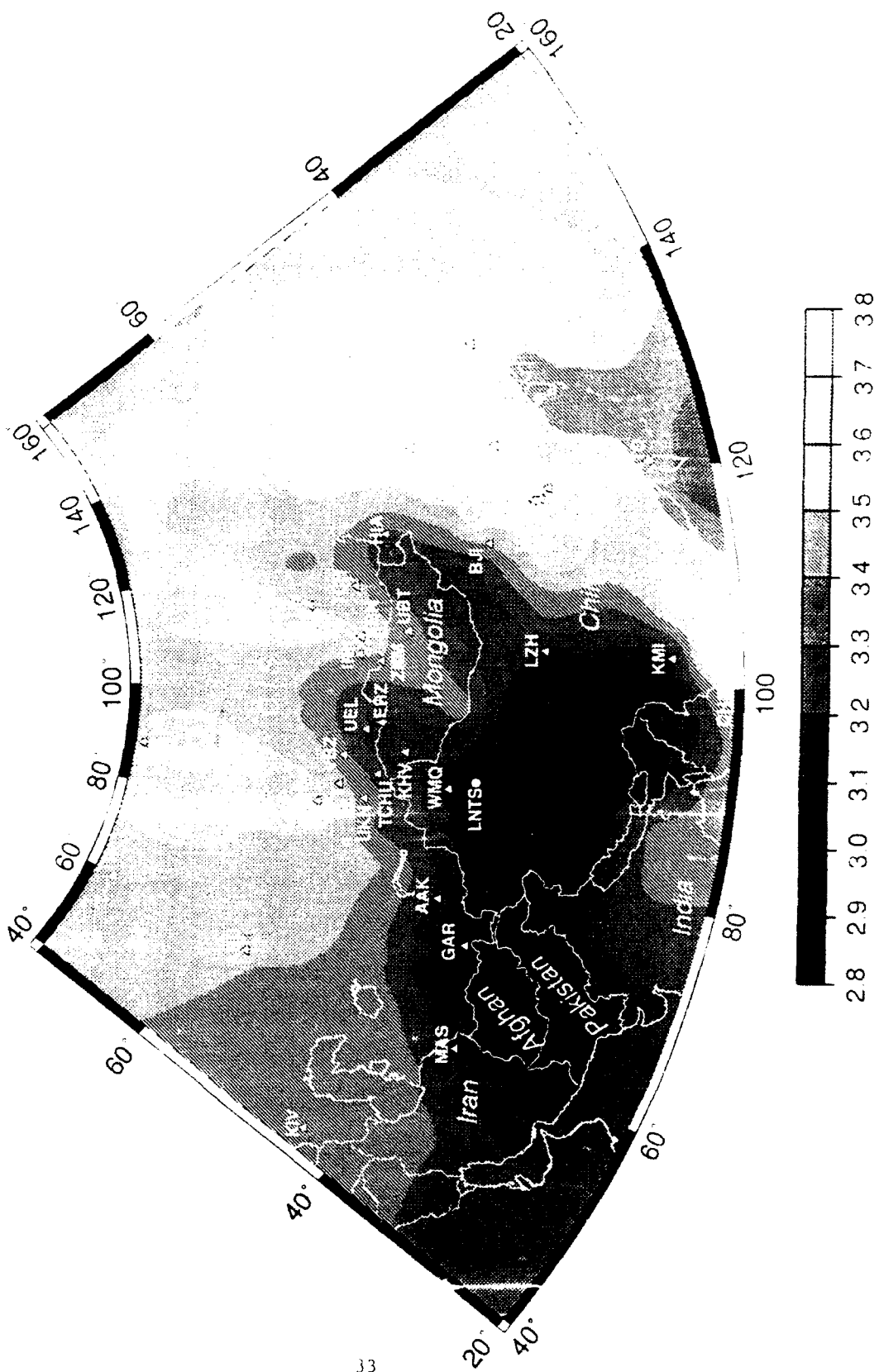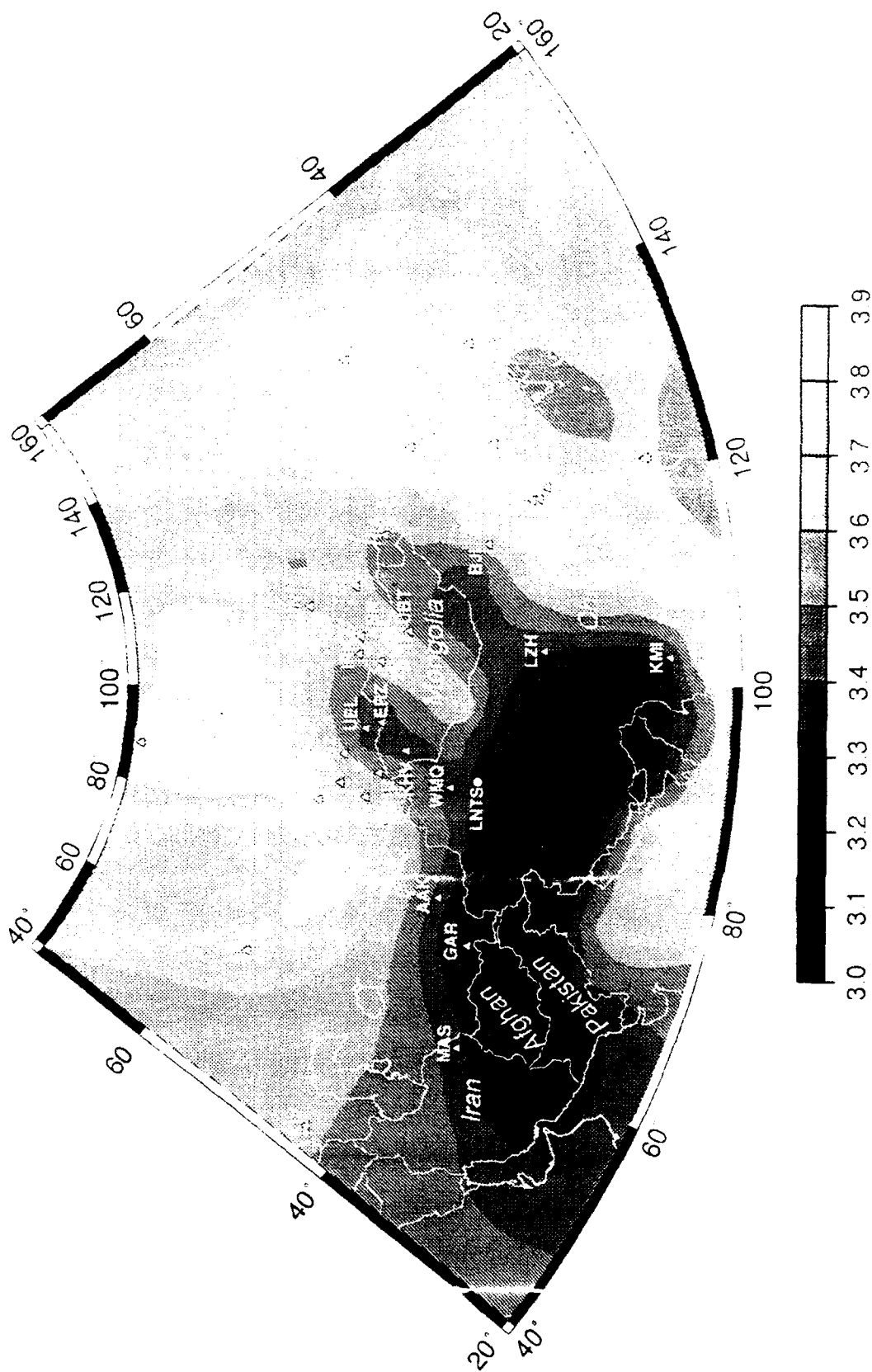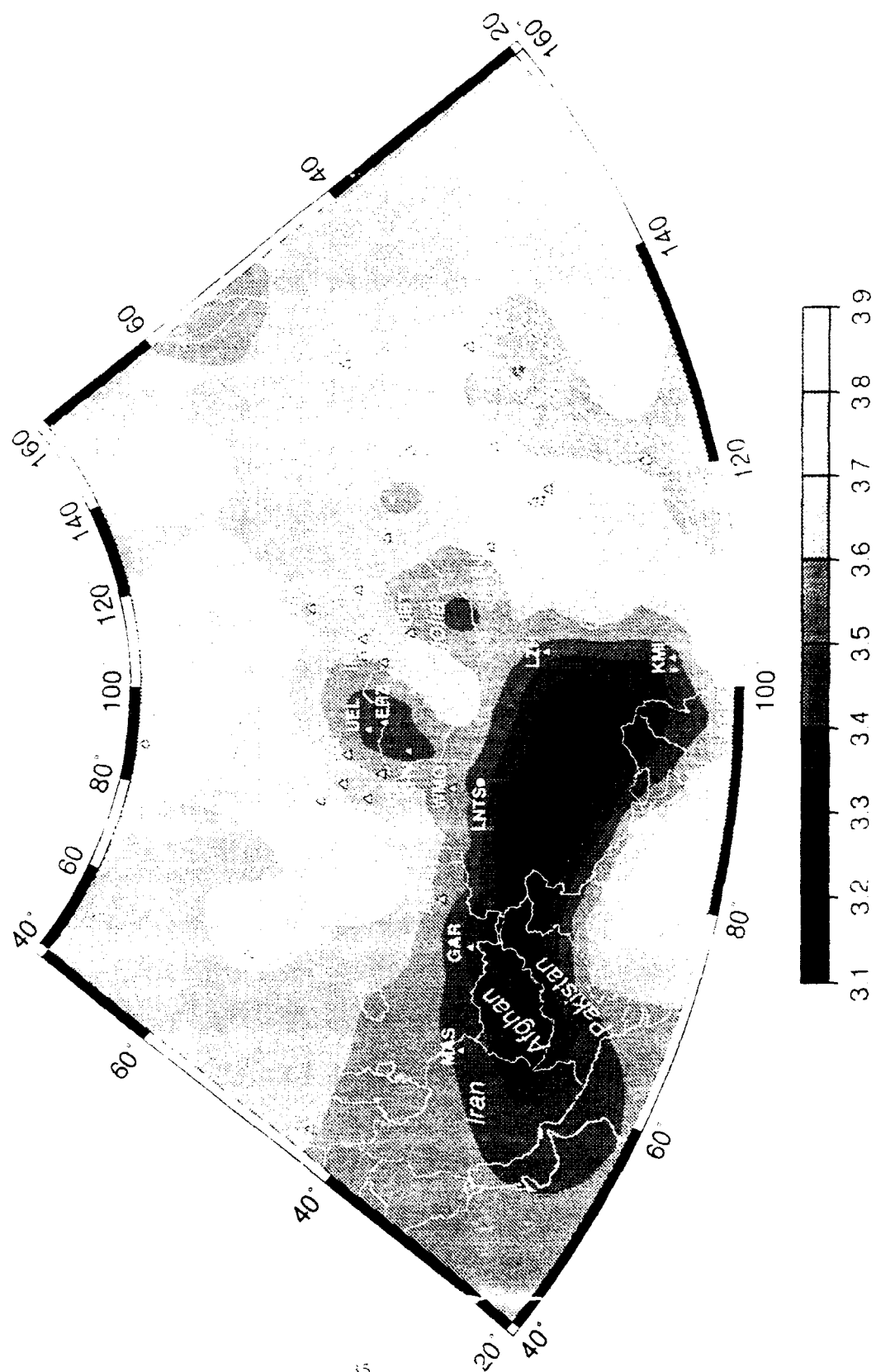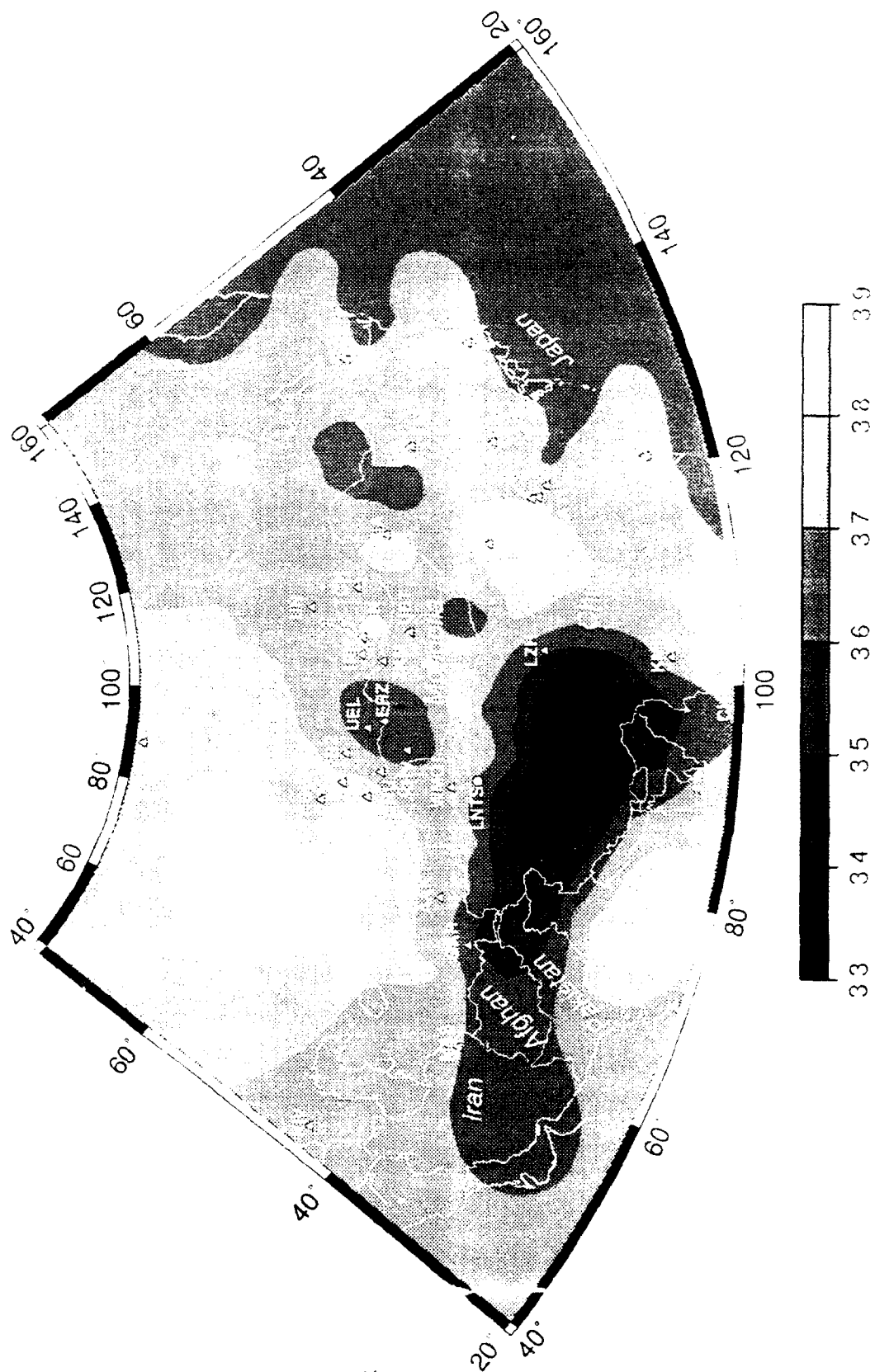
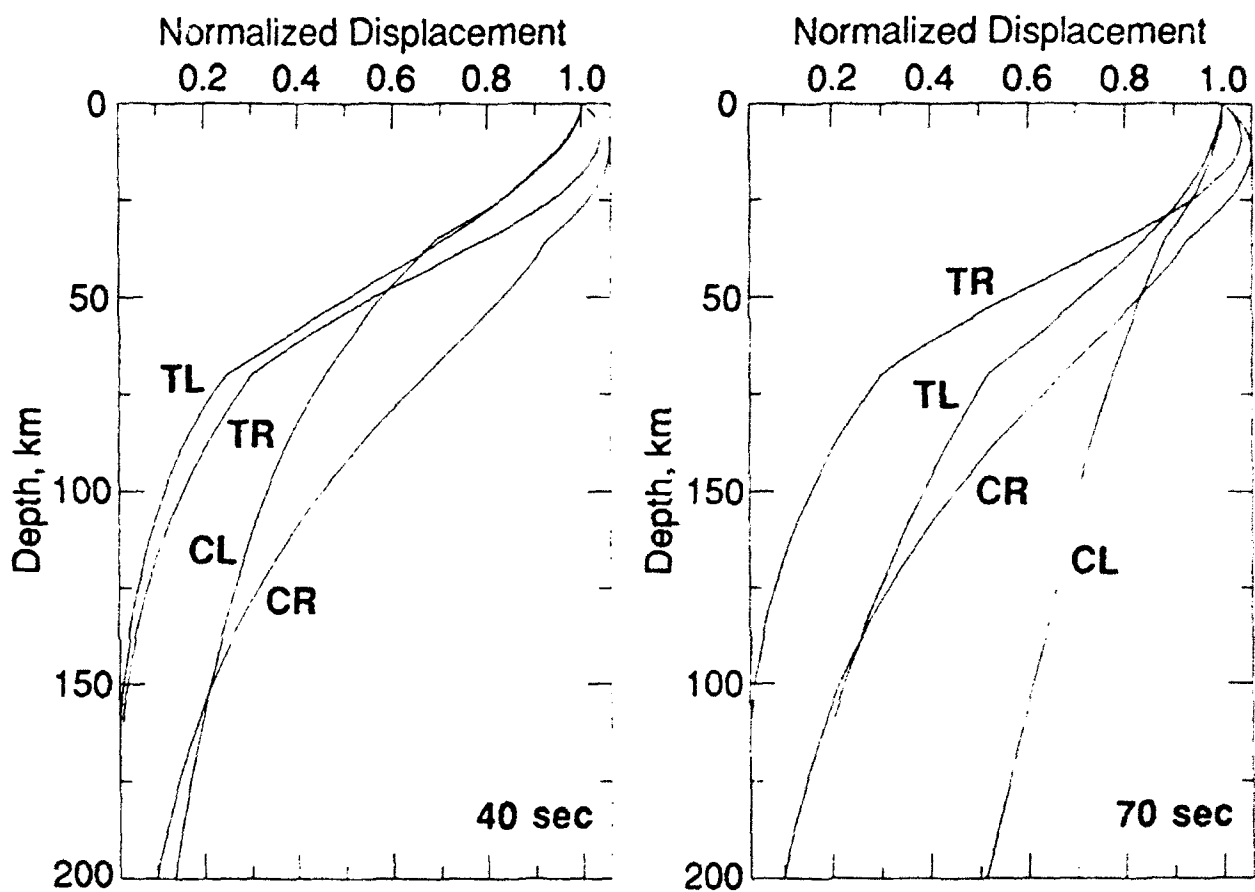Figure S6

Figure 8

Figure 4

Figure 9

Prof. Thomas Ahrens
Seismological Lab, 252-21
Division of Geological & Planetary Sciences
California Institute of Technology
Pasadena, CA 91125

Prof. Keiiti Aki
Center for Earth Sciences
University of Southern California
University Park
Los Angeles, CA 90089-0741

Prof. Shelton Alexander
Geosciences Department
403 Deike Building
The Pennsylvania State University
University Park, PA 16802

Prof. Charles B. Archambeau
CIRES
University of Colorado
Boulder, CO 80309

Dr. Thomas C. Bache, Jr.
Science Applications Int'l Corp.
10260 Campus Point Drive
San Diego, CA 92121 (2 copies)

Prof. Muawia Barazangi
Institute for the Study of the Continent
Cornell University
Ithaca, NY 14853

Dr. Jeff Barker
Department of Geological Sciences
State University of New York
 at Binghamton
Vestal, NY 13901

Dr. Douglas R. Baumgardt
ENSCO, Inc
5400 Port Royal Road
Springfield, VA 22151-2388

Dr. Susan Beck
Department of Geosciences
Building #77
University of Arizona
Tuscon, AZ 85721

Dr. T.J. Bennett
S-CUBED
A Division of Maxwell Laboratories
11800 Sunrise Valley Drive, Suite 1212
Reston, VA 22091

Dr. Robert Blandford
AFTAC/TT, Center for Seismic Studies
1300 North 17th Street
Suite 1450
Arlington, VA 22209-2308

Dr. Stephen Bratt
Center for Seismic Studies
1300 North 17th Street
Suite 1450
Arlington, VA 22209-2308

Dr. Lawrence Burdick
IGPP, A-025
Scripps Institute of Oceanography
University of California, San Diego
La Jolla, CA 92093

Dr. Robert Burridge
Schlumberger-Doll Research Center
Old Quarry Road
Ridgefield, CT 06877

Dr. Jerry Carter
Center for Seismic Studies
1300 North 17th Street
Suite 1450
Arlington, VA 22209-2308

Dr. Eric Chael
Division 9241
Sandia Laboratory
Albuquerque, NM 87185

Dr. Martin Chapman
Department of Geological Sciences
Virginia Polytechnical Institute
21044 Derring Hall
Blacksburg, VA 24061

Prof. Vernon F. Cormier
Department of Geology & Geophysics
U-45, Room 207
University of Connecticut
Storrs, CT 06268

Prof. Steven Day
Department of Geological Sciences
San Diego State University
San Diego, CA 92182

Marvin Denny
U.S. Department of Energy
Office of Arms Control
Washington, DC 20585

1

Dr. Zoltan Der
ENSCO, Inc.
5400 Port Royal Road
Springfield, VA 22151-2388


Prof. Adam Dziewonski
Hoffman Laboratory, Harvard University
Dept. of Earth Atmos. & Planetary Sciences
20 Oxford Street
Cambridge, MA 02138

Prof. John Ebel
Department of Geology & Geophysics
Boston College
Chestnut Hill, MA 02167


Eric Fielding
SNEE Hall
INSTOC
Cornell University
Ithaca, NY 14853

Dr. Mark D. Fisk
Mission Research Corporation
735 State Street
P.O. Drawer 719
Santa Barbara, CA 93102

Prof Stanley Flatte
Applied Sciences Building
University of California, Santa Cruz
Santa Cruz, CA 95064


Dr. John Foley
NER-Geo Sciences
1100 Crown Colony Drive
Quincy, MA 02169


Prof. Donald Forsyth
Department of Geological Sciences
Brown University
Providence, RI 02912


Dr. Art Frankel
U.S. Geological Survey
922 National Center
Reston, VA 22092


Dr. Cliff Frolich
Institute of Geophysics
8701 North Mopac
Austin, TX 78759

Dr. Holly Given
IGPP, A-025
Scripps Institute of Oceanography
University of California, San Diego
La Jolla, CA 92093

Dr. Jeffrey W. Given
SAIC
10260 Campus Point Drive
San Diego, CA 92121


Dr. Dale Glover
Defense Intelligence Agency
ATTN: ODT-1B
Washington, DC 20301


Dr. Indra Gupta Juan Henson
Teledyne Geotech
314 Montgomery Street
Alexanderia, VA 22314


Dan N. Hagedon
Pacific Northwest Laboratories
Battelle Boulevard
Richland, WA 99352


Dr. James Hannon
Lawrence Livermore National Laboratory
P.O. Box 808
L-205
Livermore, CA 94550


Dr. Roger Hansen
HQ AFTAC/TTR
130 South Highway A1A
Patrick AFB, FL 32925-3002


Prof. David G. Harkrider
Seismological Laboratory
Division of Geological & Planetary Sciences
California Institute of Technology
Pasadena, CA 91125


Prof. Danny Harvey
CIRES
University of Colorado
Boulder, CO 80309


Prof. Donald V. Helmberger
Seismological Laboratory
Division of Geological & Planetary Sciences
California Institute of Technology
Pasadena, CA 91125

Prof. Eugene Herrin
Institute for the Study of Earth and Man
Geophysical Laboratory
Southern Methodist University
Dallas, TX 75275

Prof. Robert B. Herrmann
Department of Earth & Atmospheric Sciences
St. Louis University
St. Louis, MO 63156

Prof. Lane R. Johnson
Seismographic Station
University of California
Berkeley, CA 94720

Prof. Thomas H. Jordan
Department of Earth, Atmospheric &
  Planetary Sciences
Massachusetts Institute of Technology
Cambridge, MA 02139

Prof. Alan Kafka
Department of Geology & Geophysics
Boston College
Chestnut Hill, MA 02167

Robert C. Kemerait
ENSCO, Inc.
445 Pineda Court
Melbourne, FL 32940

Dr. Karl Koch
Institute for the Study of Earth and Man
Geophysical Laboratory
Southern Methodist University
Dallas, Tx 75275

Dr. Max Koontz
U.S. Dept. of Energy/DP 5
Forrestal Building
1000 Independence Avenue
Washington, DC 20585

Dr. Richard LaCoss
MIT Lincoln Laboratory, M-200B
P.O. Box 73
Lexington, MA 02173-0073

Dr. Fred K. Lamb
University of Illinois at Urbana-Champaign
Department of Physics
1110 West Green Street
Urbana, IL 61801

Prof. Charles A. Langston
Geosciences Department
403 Deike Building
The Pennsylvania State University
University Park, PA 16802

Jim Lawson, Chief Geophysicist
Oklahoma Geological Survey
Oklahoma Geophysical Observatory
P.O. Box 8
Leonard, OK 74043-0008

Prof. Thorne Lay
Institute of Tectonics
Earth Science Board
University of California, Santa Cruz
Santa Cruz, CA 95064

Dr. William Leith
U.S. Geological Survey
Mail Stop 928
Reston, VA 22092

Mr. James F. Lewkowicz
Phillips Laboratory/GPEH
29 Randolph Road
Hanscom AFB, MA 01731-3010( 2 copies)

Mr. Alfred Lieberman
ACDA/VI-OA State Department Building
Room 5726
320-21st Street, NW
Washington, DC 20451

Prof. L. Timothy Long
School of Geophysical Sciences
Georgia Institute of Technology
Atlanta, GA 30332

Dr. Randolph Martin, III
New England Research, Inc.
76 Olcott Drive
White River Junction, VT 05001

Dr. Robert Masse
Denver Federal Building
Box 25046, Mail Stop 967
Denver, CO 80225

Dr. Gary McCartor
Department of Physics
Southern Methodist University
Dallas, TX 75275

Prof. Thomas V. McEvilly
Seismographic Station
University of California
Berkeley, CA 94720

Prof. John A. Orcutt
IGPP, A-025
Scripps Institute of Oceanography
University of California, San Diego
La Jolla, CA 92093

Dr. Art McGarr
U.S. Geological Survey
Mail Stop 977
U.S. Geological Survey
Menlo Park, CA 94025

Prof. Jeffrey Park
Kline Geology Laboratory
P.O. Box 6666
New Haven, CT 06511-8130

Dr. Keith L. McLaughlin
S-CUBED
A Division of Maxwell Laboratory
P.O. Box 1620
La Jolla, CA 92038-1620

Dr. Howard Patton
Lawrence Livermore National Laboratory
L-025
P.O. Box 808
Livermore, CA 94550

Stephen Miller & Dr. Alexander Florence
SRI International
333 Ravenswood Avenue
Box AF 116
Menlo Park, CA 94025-3493

Dr. Frank Pilotte
HQ AFTAC/TT
130 South Highway A1A
Patrick AFB, FL 32925-3002

Prof. Bernard Minster
IGPP, A-025
Scripps Institute of Oceanography
University of California, San Diego
La Jolla, CA 92093

Dr. Jay J. Pulli
Radix Systems, Inc.
201 Perry Parkway
Gaithersburg, MD 20877

Prof. Brian J. Mitchell
Department of Earth & Atmospheric Sciences
St. Louis University
St. Louis, MO 63156

Dr. Robert Reinke
ATTN: FCTVTD
Field Command
Defense Nuclear Agency
Kirtland AFB, NM 87115

Mr. Jack Murphy
S-CUBED
A Division of Maxwell Laboratory
11800 Sunrise Valley Drive, Suite 1212
Reston, VA 22091 (2 Copies)

Prof. Paul G. Richards
Lamont-Doherty Geological Observatory
 of Columbia University
Palisades, NY 10964

Dr. Keith K. Nakanishi
Lawrence Livermore National Laboratory
L-025
P.O. Box 808
Livermore, CA 94550

Mr. Wilmer Rivers
Teledyne Geotech
314 Montgomery Street
Alexandria, VA 22314

Dr. Carl Newton
Los Alamos National Laboratory
P.O. Box 1663
Mail Stop C335, Group ESS-3
Los Alamos, NM 87545

Dr. George Rothe
HQ AFTAC/TTR
130 South Highway A1A
Patrick AFB, FL 32925-3002

Dr. Bao Nguyen
HQ AFTAC/TTR
130 South Highway A1A
Patrick AFB, FL 32925-3002

Dr. Alan S. Ryall, Jr.
DARPA/NMRO
3701 North Fairfax Drive
Arlington, VA 22209-1714

Dr. Richard Sailor
TASC, Inc.
55 Walkers Brook Drive
Reading, MA  01867

Prof. Charles G. Sammis
Center for Earth Sciences
University of Southern California
University Park
Los Angeles, CA  90089-0741

Prof. Christopher H. Scholz
Lamont-Doherty Geological Observatory
 of Columbia University
Palisades, NY  10964

Dr. Susan Schwartz
Institute of Tectonics
1156 High Street
Santa Cruz, CA  95064

Secretary of the Air Force
(SAFRD)
Washington, DC  20330

Office of the Secretary of Defense
DDR&E
Washington, DC  20330

Thomas J. Sereno, Jr.
Science Application Int'l Corp.
10260 Campus Point Drive
San Diego, CA  92121

Dr. Michael Shore
Defense Nuclear Agency/SPSS
6801 Telegraph Road
Alexandria, VA  22310

Dr. Robert Shumway
University of California Davis
Division of Statistics
Davis, CA  95616

Dr. Matthew Sibol
Virginia Tech
Seismological Observatory
4044 Derring Hall
Blacksburg, VA  24061-0420

Prof. David G. Simpson
IRIS, Inc.
1616 North Fort Myer Drive
Suite  1050
Arlington, VA  22209

Donald L. Springer
Lawrence Livermore National Laboratory
L-025
P.O. Box 808
Livermore, CA  94550

Dr. Jeffrey Stevens
S-CUBED
A Division of Maxwell Laboratory
P.O. Box 1620
La Jolla, CA  92038-1620

Lt. Col. Jim Stobie
ATTN: AFOSR/NL
110 Duncan Avenue
Bolling AFB
Washington, DC  20332-0001

Prof. Brian Stump
Institute for the Study of Earth & Man
Geophysical Laboratory
Southern Methodist University
Dallas, TX  75275

Prof. Jeremiah Sullivan
University of Illinois at Urbana-Champaign
Department of Physics
1110 West Green Street
Urbana, IL  61801

Prof. L. Sykes
Lamont-Doherty Geological Observatory
 of Columbia University
Palisades, NY  10964

Dr. David Taylor
ENSCO, Inc.
445 Pineda Court
Melbourne, FL  32940

Dr. Steven R. Taylor
Los Alamos National Laboratory
P.O. Box 1663
Mail Stop C335
Los Alamos, NM  87545

Prof. Clifford Thurber
University of Wisconsin-Madison
Department of Geology &  Geophysics
1215 West Dayton Street
Madison, WS  53706

5

Prof. M. Nafi Toksoz
Earth Resources Lab
Massachusetts Institute of Technology
42 Carleton Street
Cambridge, MA 02142

Dr. Larry Turnbull
CIA-OSWR/NED
Washington, DC 20505

Dr. Gregory van der Vink
IRIS, Inc.
1616 North Fort Myer Drive
Suite 1050
Arlington, VA 22209

Dr. Karl Veith
EG&G
5211 Auth Road
Suite 240
Suitland, MD 20746

Prof. Terry C. Wallace
Department of Geosciences
Building #77
University of Arizona
Tuscon, AZ 85721

Dr. Thomas Weaver
Los Alamos National Laboratory
P.O. Box 1663
Mail Stop C335
Los Alamos, NM 87545

Dr. William Wortman
Mission Research Corporation
8560 Cinderbed Road
Suite 700
Newington, VA 22122

Prof. Francis T. Wu
Department of Geological Sciences
State University of New York
 at Binghamton
Vestal, NY 13901

AFTAC/CA
(STINFO)
Patrick AFB, FL 32925-6001

ARPA, OASB/Library
3701 North Fairfax Drive
Arlington, VA 22203-1714

HQ DNA
ATTN: Technical Library
Washington, DC 20305

Defense Intelligence Agency
Directorate for Scientific & Technical Intelligence
ATTN: DTIB
Washington, DC 20340-6158

Defense Technical Information Center
Cameron Station
Alexandria, VA 22314 (2 Copies)

TACTEC
Battelle Memorial Institute
505 King Avenue
Columbus, OH 43201 (Final Report)

Phillips Laboratory
ATTN: XPG
29 Randolph Road
Hanscom AFB, MA 01731-3010

Phillips Laboratory
ATTN: GPE
29 Randolph Road
Hanscom AFB, MA 01731-3010

Phillips Laboratory
ATTN: TSML
5 Wright Street
Hanscom AFB, MA 01731-3004

Phillips Laboratory
ATTN: PL/SUL
3550 Aberdeen Ave SE
Kirtland, NM 87117-5776 (2 copies)

Dr. Michel Bouchon
I.R.I.G.M.-B.P. 68
38402 St. Martin D'Heres
Cedex, FRANCE

Dr. Michel Campillo
Observatoire de Grenoble
I.R.I.G.M.-B.P. 53
38041 Grenoble, FRANCE

6

Dr. Kin Yip Chun
Geophysics Division
Physics Department
University of Toronto
Ontario, CANADA

Prof. Hans-Peter Harjes
Institute for Geophysic
Ruhr University/Bochum
P.O. Box 102148
4630 Bochum 1, GERMANY

Prof. Eystein Husebye
NTNF/NORSAR
P.O. Box 51
N-2007 Kjeller, NORWAY

David Jepsen
Acting Head, Nuclear Monitoring Section
Bureau of Mineral Resources
Geology and Geophysics
G.P.O. Box 378, Canberra, AUSTRALIA

Ms. Eva Johannisson
Senior Research Officer
FOA
S-172 90 Sundbyberg, SWEDEN

Dr. Peter Marshall
Procurement Executive
Ministry of Defense
Blacknest, Brimpton
Reading FG7-FRS, UNITED KINGDOM

Dr. Bernard Massinon, Dr. Pierre Mechler
Societe Radiomana
27 rue Claude Bernard
75005 Paris, FRANCE (2 Copies)

Dr. Svein Mykkeltveit
NTNT/NORSAR
P.O. Box 51
N-2007 Kjeller, NORWAY (3 Copies)

Prof. Keith Priestley
University of Cambridge
Bullard Labs, Dept. of Earth Sciences
Madingley Rise, Madingley Road
Cambridge CB3 OEZ, ENGLAND

Dr. Jorg Schlittenhardt
Federal Institute for Geosciences & Nat'l Res.
Postfach 510153
D-3000 Hannover 51, GERMANY

Dr. Johannes Schweitzer
Institute of Geophysics
Ruhr University/Bochum
P.O. Box 1102148
4360 Bochum 1, GERMANY

Trust & Verify
VERTIC
8 John Adam Street
London WC2N 6EZ, ENGLAND